Modeling deltaic response to changes in fluvial sediment delivery

By Jaap Nienhuis on September 4, 2011

Supervisors:
Suzanne Hulscher
Pieter Roos
Andrew Ashton

1 Summary

River deltas are extremely dynamic and complex depositional features, shaped by marine and fluvial processes. Due to growing social, environmental and economic pressures, such as population growth and sea level rise, understanding of these systems becomes increasingly relevant. This study aims at identifying and characterizing long-term (centennial) deltaic response to changes in fluvial sediment load. Two types of changes are distinguished: (i) permanent elimination of the sediment supply and (ii) time periodic sediment supply. Thus: how does the shoreline of a wave-dominated delta develop having time-periodic or elimination of fluvial sediment delivery?

A numerical model utilizes the relation between waves and littoral transport to calculate shoreline displacement. Aimed at studying wave-dominated deltas, the addition of fluvial sediment somewhere along the shore builds a delta.

(i) The directionality and energy of waves determines to a large extent how a delta develops after the elimination of fluvial sediment supply. There are four distinct modes in which a wave-dominated delta can be abandoned. A diffusive mode erodes deposits near the river mouth. Higher wave direction asymmetry creates a discontinuity that propagates downdrift after elimination of riverine sediment input. One of these modes creates a spit that erodes large portions of the shoreline. The Ebro delta, Spain, is an example of that mode. The current shape of these spits can reveal the abandonment conditions of historical lobes. Large trains of downdrift sandwaves before and after lobe abandonment characterize a sandwave-mode.

(ii) More regular variation in fluvial input influences downdrift migrating sandwaves. The frequency and magnitude of the riverine "forcing" can initiate an equal pattern that migrates away from the river mouth. There exists a select range of climate forcing frequencies and magnitudes in which that translation is one-to-one. Longer period signals are shredded by autogenic-formed sand waves. Input variation also affects the depositional structure of the delta. Unstable downdrift shorelines, such as the time-periodic megadroughts that influence the Godavari delta, have a highly non-linear response on input signals. The coupling of input signals with updrift deposition is much simpler. Regular updrift erosion creates convex beach ridges up to a distance that is determined by the riverine variation.

Understanding and recognizing these conditions helps determine the style and results of historical, current and future delta evolution.

Contents

2 Introduction

River deltas are among the world's most fertile and densely populated regions. Almost half a billion people live on or near deltas. These regions are also geologically extremely dynamic, affected by, among others, human river basin interventions and climate change on top of any autogenic variability. Current issues arise from river damming, sea level rise and excessive water use.

Unraveling the morphodynamical processes that shape these regions is both of scientific as well as practical interest. Part in understanding the behavior of these complex features is to investigate their response to various forcing mechanisms. To relate effects of different processes, quantification is important. Fundamental, physics-based research can create a framework for more detailed and local analyses.

This study focuses on the effects of changes in fluvial sediment supply. River damming, climate variability and river avulsions can dramatically influence riverine input. Societal and environmental pressures will make these factors increasingly important for the coming generations.

Two scenarios are picked: deltaic response to fluvial input elimination and deltaic response to regular fluvial input variation. This is extended into 2 scenarios using marine data: Lobe abandonment at the Ebro delta (Spain) and deposition of fluvial variations on the Godavari delta (India). The Ebro delta is chosen because of two separate lobes that experienced input elimination. Long-term time-periodic fluctuation in sediment supply characterizes the monsoon-fed Godavari delta.

The selective treatment of physical processes, only wave sustained littoral transport is included, make this research most applicable to wave-dominated deltas. Note that, throughout this report, wave climate refers to the angular distribution and energy flux of the incoming waves.

A brief overview of modern research into delta development is given in chapter 3, with aims of this research in chapter 4. Chapter 5 treats the research methods used. Results are discussed in chapters 6 through 9. Discussion and conclusions are stated in chapter 10.

2.1 Objective

The objective of this study is:

"To investigate the effect of fluvial sediment supply changes on wave-influenced delta morphodynamics."

3 Background

The objective stated in section 2.1 allows us to treat the theory of two topics, namely delta formation (section 3.1) and the origin of fluvial sediment supply fluctuations (section 3.2).

3.1 Delta formation

Suter [1997] defined a delta as a "coastal accumulation of sediment extending both above and below sea level, formed where a river enters an ocean or other large body of water". A trivial environmental requirement is the (historical) presence of a river mouth. Holocene sea level rise has reshaped this location. If there is a retreat of the river, a drowned river valley forms an estuary. Where fluvial sediment input can "keep up" with this rise, a delta develops [*Dalrymple et al.*, 1992].

A large number of different environmental controls exist that determine the delta shape. Galloway [1975] recognized river discharge, tidal range and wave energy flux as having a first order morphologic control. Other reported influences are: grain size distribution [*Orton and Reading*, 1993], (relative) sea level rise [*Giosan et al.*, 2006], human engineering [*Syvitski et al.*, 2009], sediment cohesion [*Edmonds and Slingerland*, 2010] and wave climate [*Ashton and Giosan*, 2011].

Sediment delivery through the river mouth is the primary control on deltaic deposition. A decreasing flow velocity of the stream creates sedimentation of the marine basin. Suspended sediment is carried furthest, creating a deltaic *bottomset*. Bedload settles near the river mouth and redistributes in crossshore direction via slope processes, resulting in a *foreset*. Fluvial dynamics upstream deposits fine *topset* material [*Wright*, 1977]. Figure 3-1 shows a characteristic outline of this stratigraphy.

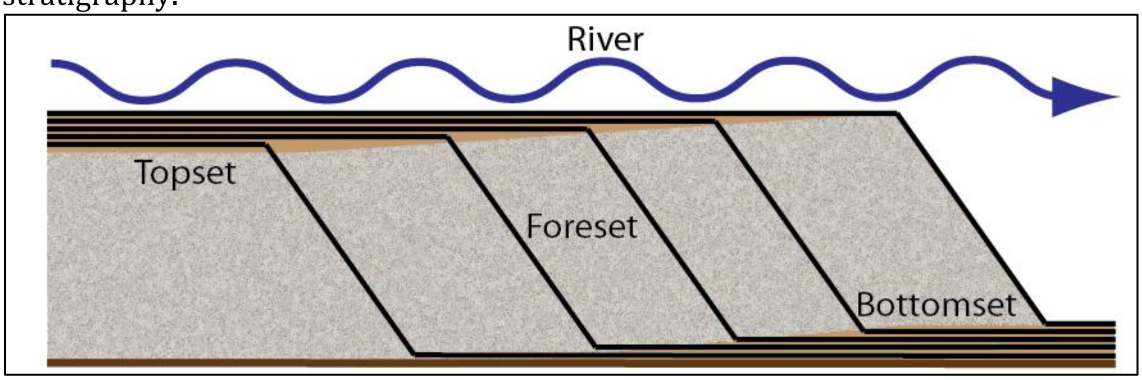

Figure 3-1: Classic Gilbert-type (coarse grained) cross section. A side view: the delta expands to the right.

This section treats deltaic morphodynamics along three main drivers: fluvial, tidal and wave-driven processes.

3.1.1 Fluvially-induced morphodynamics

Starting at the river mouth, several distinct characteristics of the fluvio-marine interaction determine the resulting morphology.

Bates [1953] classified different types of river mouths based on dominant physical mechanisms:

A. Buoyancy of riverine (fresh) water on the marine (salt) water.
B. Friction of the marine bed on the outflowing water
C. Momentum (inertia) of the riverine outflow into the marine basin

Type B and C rivermouths (friction/momentum-dominated) build natural levees. High velocity differences at the jet edges disperse the sediment. Settling at these edges removes sediment from the jet center, limiting deposition downstream [*Rowland et al.*, 2010]. The river mouth (and thus the delta) progrades into the marine basin due to continuous levee building and flow channeling [*Anderson and Anderson*, 2011].

Another morphodynamic feature of these river mouths is the deposition of a mouth bar. Sediment settles downstream of the jet at the steepest gradient in sediment flux (minimum in divergence). The mouth bar migrates downstream (like a river dune) until it reaches a critical height, when the flow is pushed around rather than over the bar [*Edmonds and Slingerland*, 2007]. This competition between levee building and bar formation eventually bifurcates the river.

Another way in which fluvially induced morphodynamics shape a delta is via upstream avulsion. As the river progrades, it increases the difference between crossshore and alongshore surface-slope. Lateral channel migration, meandering, is a mechanism which spreads sediment. Natural levees control lateral spreading, if avulsion is the "dominant mechanism of lateral channel motion" [*Jerolmack and Mohrig*, 2007]. The upstream location where this breaching preferably occurs scales with the backwater length, being an order of magnitude larger than flow bifurcation [*Jerolmack and Mohrig*, 2007]. Figure 2-2 shows a typical river dominated delta network. Breaching and building of different delta lobes is part of a larger framework known as the Delta Cycle [*Roberts*, 1997]. This cycle describes the phases of a deltaic lobe, starting from initial sedimentation of a marine basin to the subsidence and marine reworking of its subaerial surface. This autogenic variation creates large changes in the sediment load delivered to a specific lobe.

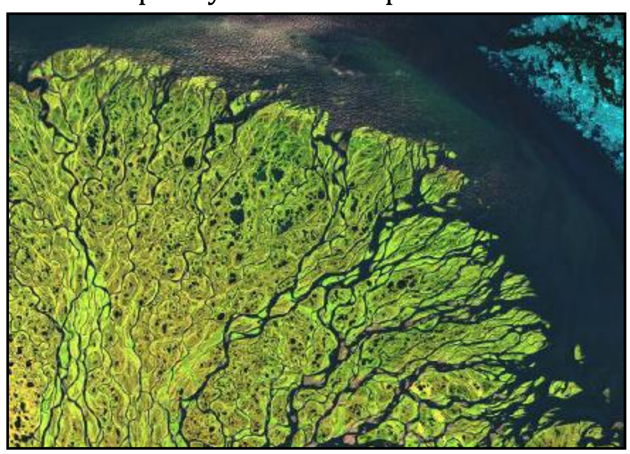

Figure 3-2: Lena River, Russia. A river dominated delta [*Huh et al.*, 2004]. The area depicted is about 100km by 60km.

3.1.2 Tide-induced morphodynamics

The continuous movement of sediment and water up and down the river mouth influences processes discussed earlier. There is a larger fluvio-marine interaction zone, carrying sediment up- and downstream. Tides tend to form multiple parallel ridges, formed similarly to a mouth bar [*Wright*, 1977].

Figure 3-3: Typical tide-dominated delta with multiple active channels. Ganges-Brahmaputra River, Bangladesh [*Huh et al.*, 2004]. The image comprises about 200km by 130km.

Increased downstream discharge maintains a greater number of distributaries due to the "flushing" of old channels that would have been abandoned in a river-dominated setting [*Fagherazzi*, 2008]. In fact, Fagherazzi [2008] hypothesized a self maintained criticality of the amount of active channels. Abandonment of channels increases the tidal prism through other channels. A low tidal flux eliminates the channel closest to siltation [*Fagherazzi*, 2008]. Figure 2-3 shows a tide-dominated delta.

3.1.3 Wave-induced morphodynamics

Waves also affect delta morphology. Close to the river mouth, waves reduce outflow momentum and increase vertical and horizontal mixing. Waves tend to laterally spread the river mouth bar and to constrict the outlet, reducing the number of bifurcations and flattening the shoreline [*Jerolmack and Swenson*, 2007; *Wright*, 1977]. The actual morphodynamics resulting from the interaction between waves and the river mouth is poorly understood [*Edmonds and Slingerland*, 2007].

Figure 3-4: Baram River, Malaysia. A prototype wave dominated delta [*Huh et al.*, 2004]. The area is about 150km by 100km.

Littoral transport, driven by waves, also influences mouth bar dynamics. Subaerial mouth bars can migrate and form spits that grow with the direction of littoral transport, shadowing portions of the downdrift delta. This transport also generally deflects the river mouth away from the dominant wave direction [*Giosan*, 2007]. Pranzini [*Pranzini*, 2001] showed that growing wave influenced deltas can migrate towards the waves, when updrift sediment changes its transport direction and becomes larger than downdrift transport.

On larger scales waves, which drive alongshore transport of sediment, modify the shape of the delta. Grijm [1964] and Bakker [1965] provided analytical solutions of the combined effect of fluvial sediment supply and littoral transport. Using the one-line concept, they derived equilibrium states of stable (cuspate) deltaic shorelines. Komar [1973] expanded upon this research by creating a computer model. In general, the wave energy flux determines the speed of the diffusion process, acting upon a beach section. Higher energy waves therefore generally decrease the plan-view extent of the delta.

An oblique wave approach forms an asymmetrical delta [*Bhattacharya and Giosan*, 2003], having an increased probability on downdrift spits and shoreline instability [*Ashton and Giosan*, 2011]. Asymmetry in the wave climate can also cause a morphodynamic groyne effect, where sediment is preferably deposited updrift [*Ashton and Giosan*, 2011]. Due to a low aspect ratio, avulsions are rarer. Figure 2-4 shows a delta reworked by waves.

3.2 Fluvial sediment supply changes

The focus of this report is on two types of changes; fluvial input elimination and time-periodic fluvial input. This section provides a brief summary of possible causes, which can be both autogenic (a property of the deltaic system itself) and allogenic (forced by external conditions).

Autogenic elimination of sediment delivery is for example due to lobe switching [*Roberts*, 1997]; allogenic sources can be due to climate or human river basin interventions [*Milliman et al.*, 2008].

Historically, deforestation of river basins, increasing erosion, initially spurred an increase in sediment delivery. In Europe, this is shown to have greatly increased deltaic area in the last millennium [*Giosan*, personal communication]. River damming, starting in the 20th century, dramatically decreases sediment delivery [*Syvitski et al.*, 2009]. A large portion of suspended load settles in the engineered reservoir, while most of the time all the bedload is retained. Two factors influence the flow downstream; if water flows remain sufficient to transport water, erosion occurs on the river bed, causing ecological and geomorphologic degradation. The river bed suffers from sedimentation is flows become too small. The Nile delta, where erosion is up to 150m of shoreline per year, is a dramatic example of effects from dam construction [*Vericat and Batalla*, 2006]. Irrigation, limiting discharge downstream, has also decreased sediment transport [*Ericson et al.*, 2006].

There are numerous other threats to deltaic environments, such as increased subsidence and soil salinity [*Syvitski and Saito*, 2007]. These are not in the scope of this research.

The most obvious time-periodic fluctuation in sediment delivery is seasonal variation. On longer time-scales (O (10^1-10^2) years), it is believed that monsoon driven rivers exhibit variability in their sediment load. Periods with an increased probability on monsoon failure and megadroughts drive this variation [*Giosan,* personal communication]. Variation can also be driven by autogenic riverine processes [*Jerolmack and Paola*, 2010].

There have been few studies looking at the relation between regular long term sediment supply fluctuations and plan view delta evolution. Fraticelli [2006] investigated the ridge-trough architecture and its relation to El Nina and El Nino events for the Brazos delta, Texas. On somewhat smaller temporal and spatial scales, she found a clear link between past climate and the formation of ridges on the downdrift side of the delta.

4 Aims

Knowing about effect of waves on the development of deltaic shorelines under static environmental conditions (i.a. [*Ashton and Giosan*, 2011; *Jerolmack and Swenson*, 2007]); this research will focus on the effect of fluvial change on wave-dominated deltas.

Several specific, relevant scenarios will address this objective:

1. Deltaic response to fluvial input elimination (chapters 6 & 7)
    a. How does the wave climate set the lobe abandonment regime?
    b. How is lobe abandonment embedded into delta morphology: some perspectives on the Ebro Delta
2. Deltaic response to fluvial input variation (chapters 8 & 9)
    a. How does fluvial variability affect autogenic shoreline instability?
    b. How do large climate fluctuations imprint themselves onto deltaic morphological history: some perspectives on the Godavari Delta

5 Method

This section discusses a selection of the methods used in this study. Section 1 treats the numerical model. Section 2 and 3 consider respectively its input and output. Section 4 treats some previous model results.

5.1 Model

The model used in this study is a one-contour-line cellular shoreline model, described in detail in Ashton & Murray [2006b].[1] Its purpose is exploratory [*Murray*, 2003], studying the effect of a limited number of physical processes on shoreline behavior. It does so by relating the direction and magnitude of incoming waves to the amount of transported sediment in the littoral zone.

5.1.1 Morphodynamics

Assuming that littoral transport is confined close to the shore, erosion or accretion of the shore is proportional to the derivative of this transport. The model uses this approach to calculate fluxes of sediment and subsequent shoreline orientation across computational cells. Adding "fluvial" sediment in a cell at a predefined position along the shore simulates the plan view evolution of a wave-dominated delta [*Ashton and Giosan*, 2011]. The governing sediment continuity (Exner) equation is the following (1), where a gradient in littoral transport ($\frac{\partial Q_s}{\partial x}$) ($m^3s^{-1}m^{-1}$) is set equal to accretion or erosion ($\frac{\partial \eta}{\partial t}$) ($ms^{-1}$) of the local shoreline volume D (m). The function $f(x,t)$ (m^2s^{-1}) represents the spatial and temporal local fluvial sediment flux (see subsection 5.2.1).

$$D \cdot \frac{\partial \eta}{\partial t} + \frac{\partial Q_s}{\partial x} = f(x,t) \tag{1}$$

Littoral transport is calculated via the CERC-formula, relating the direction and energy of the breaking waves to the littoral transport [*Ashton and Murray*, 2006b] (2). K_1 is an empirical constant, which can vary greatly between different sediment types. H_b is the breaking wave height. φ_b - ϑ is the difference between the direction of incoming waves (φ_b) and the shoreline orientation (ϑ).

$$Q_s = K_1 \cdot {H_b}^{\frac{5}{2}} \cdot \cos(\varphi_b - \vartheta) \cdot \sin(\varphi_b - \vartheta) \tag{2}$$

There exist alongshore variations in breaking wave height, due to undulations in the plan view shoreline. Within this model, the equation above can be restated into deepwater wave conditions (3).

$$Q_s = K_2 \cdot {H_0}^{\frac{12}{5}} \cdot T^{\frac{1}{5}} \cdot \cos^{\frac{6}{5}}(\varphi_0 - \vartheta) \cdot \sin(\varphi_0 - \vartheta) \tag{3}$$

[1] There are some innovations in the model since Ashton & Murray [2006b] (i.a. fluvial input, multiple deltaic lobes, rocky shorelines, multi-processor core support)

K_2 is an empirical constant (ms^{-2}), relating wave energy to sediment volume; H_0 and T are respectively the significant deepwater waveheight and waveperiod. The (spatial) gradient of this transport can be mapped to the Exner equation (1), yielding a nonlinear diffusion equation [*Ashton and Murray*, 2006b] (4):

$$\frac{\partial \eta}{\partial t} = -\frac{K_2}{D} \cdot {H_0}^{\frac{12}{5}} \cdot T^{\frac{1}{5}} \cdot \psi \cdot \frac{\partial^2 \eta}{\partial x^2} \tag{4}$$

Where:

$$\psi = \cos^{\frac{1}{5}}(\varphi_0 - \vartheta) \cdot \left[\cos^2(\varphi_0 - \vartheta) - (\frac{6}{5})\sin^2(\varphi_0 - \vartheta)\right] \tag{5}$$

Ψ, dependent on the relative angle of incoming waves, determines whether the shoreline is stable (negative diffusion coefficient) or unstable (positive shoreline coefficient). Figure 5-1a shows littoral sediment transport and the diffusion coefficient as a function of the wave approach angle. The maximizing angle for sediment transport using the CERC formula is 42^0 [*Komar*, 1998], where the diffusion coefficient shifts from negative to positive.

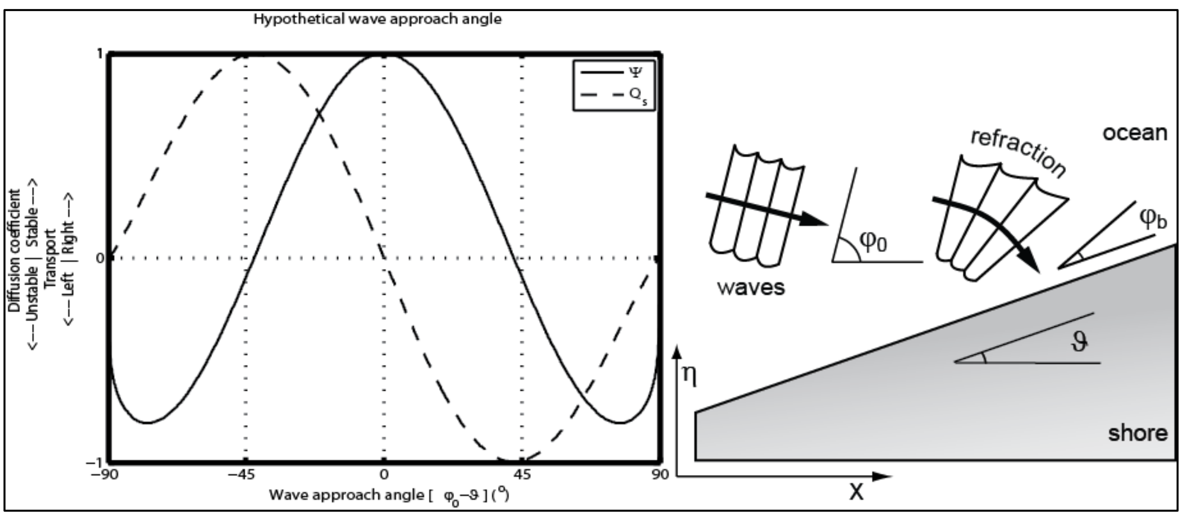

Figure 5-1: Sediment transport and diffusion with various wave approach angles.

5.1.2 Domain

The coastal zone surface is discretized into square cells, with sides of 200m for most simulations. A value F describes the portion of subaerial surface of each cell, being between 0 and 1 if the cell is part of a shoreline. If F equals 1, the cell consists entirely of "land". Figure 5-2a shows an annotated example shoreline. The algorithm uses F to trace the location and orientation of the shore within a cell. Location is a fraction of the cell length perpendicular to the subaerial neighbor. The position of the shore to the "left" and "right" determines the orientation [*Ashton and Murray*, 2006b].

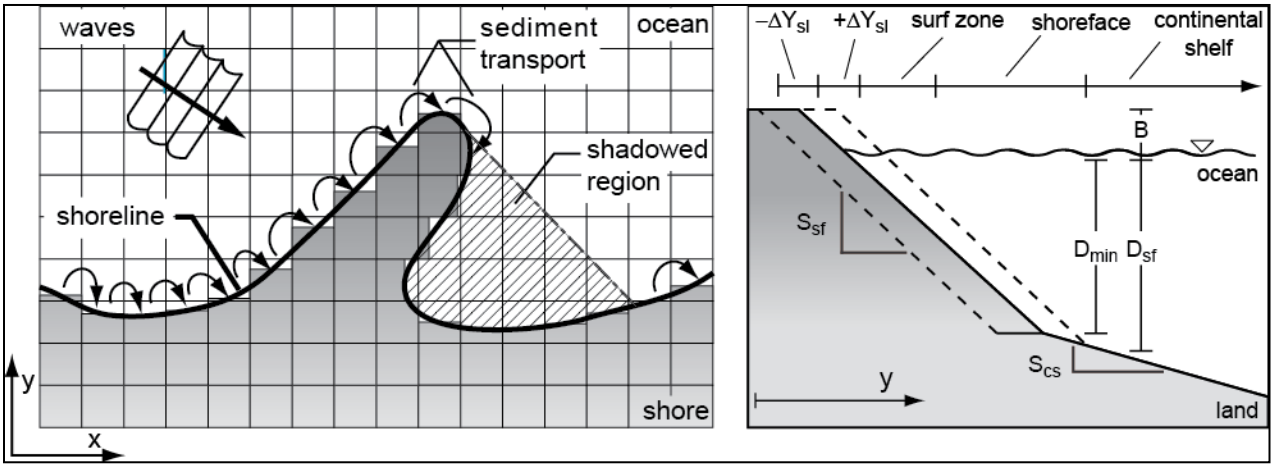

Figure 5-2: Model domain explained. Copied from: [*Ashton and Murray*, 2006b].

Left and right domain boundaries are periodic; sand transported over the rightmost cell, enters the domain from the left. All simulations start with a straight shoreline. Cross-shore erosion and deposition is explained in Figure 5-2b. Deposition occurs evenly throughout the shoreface, up until D_{sf}, where the shoreface gradient (S_{sf}) intersects the gradient of the continental shelf (S_{cs}). Erosion maintains a minimum shoreface depth (D_{min}).

5.1.3 Algorithm

Each timestep, set at 1 day for all simulations, a random number between 0 and 1 is picked. This number is used to "draw" a wave direction from the cumulative probability distribution extracted from the wave climate. Other wave characteristics are set constant in the simulations. Deepwater waves are then refracted over parallel depth contours. The local shoreline orientation then determines the sediment transport across neighboring shoreline cells, utilizing the CERC-equation at breaking wave conditions [*Komar*, 1998]. A shadow routine searches for cells on the shoreline hidden from the current wave direction. Transport out of those cells is set to zero. Barrier overwash transports sediment over a spit, maintaining a minimum barrier width [*Ashton and Murray*, 2006b].

Fluvial sediment transport is converted to the fraction F, updating each cell with the appropriate amount. The cell which contains the river mouth is updated with the fluvial bedload at each timestep. The numerical scheme can become unstable, when the combination of cell size and time step does not meet the Courant-condition.

5.1.4 Assumptions

This exploratory model is designed for large-scale coastal evolution, spatial scales larger than a couple cells and temporal scales at least longer than a year [*Ashton and Murray*, 2006b; *de Vriend et al.*, 1993; *Murray*, 2003]. Neglecting cross-shore transport results in minor discrepancies since the delta and its morphodynamic features are orders of magnitude larger than the littoral zone [*Murray and Ashton*, 2004]. It is assumed that smaller scale shoreline features are superimposed on (and therefore are not affecting) a general trend. Shore parallel depth contours neglects convergence and divergence of wave energy on an undulating shore. This is "allowed" if the alongshore scale is much larger than the cross-shore extent [*Falqués and Calvete*, 2005]. Violating this assumption, by extending to far onto the shelf, over-predicts the angle of incoming waves. Furthermore, perturbation theory suggests the requirement of a minimum shoreline length and a minimum cross shore extent for perturbations to grow [*Falqués and Calvete*, 2005].

The fluvial environment is simplified by placing the transported bedload on to the shore. Although suspended load (smaller grains) affects sedimentation, bedload is primarily responsible for longer timescale delta development [*Orton and Reading*, 1993].

For simplicity, lobes are modeled with the river mouth location predefined alongshore. There is no feedback between the course of the river and the dynamics of the shoreline. The combination of the primary modeled process (littoral transport) and other processes would make the importance of externally set conditions difficult to interpret. The model would quickly lose its physical character.

5.2 Input

This section discusses the translation of the fluvial and marine environment into model controls.

5.2.1 Fluvial environment

The riverine input is based upon three parameters: a period (in years), amplitude (in %) and average load (in kgs^{-1}). The amplitude is determined as a fraction of the average load. See Figure 5-3.

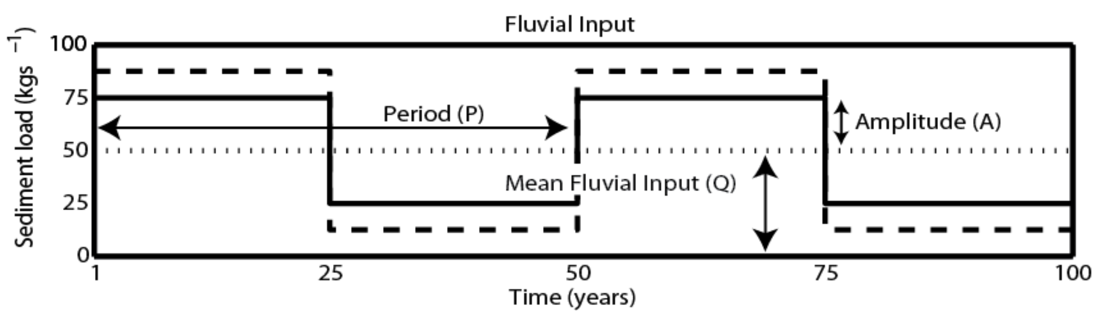

Figure 5-3: Setting the sediment load record. Solid line: Q50, P50, A50. Dashed line: Q50, P50, A80.

Hoogendoorn et al. [2008] investigated the effect of supply variation of delta clinoform. They modeled variation as the sum of a fixed and a random discharge component. This study will not use such an approach because the randomness must be orders of magnitude smaller in frequency than the desired scale of the results.

5.2.2 Marine environment

The marine environment is modeled as a distribution of deepwater wave energy. This distribution translates in a probability density function from which random waves are generated in the model. Figure 5-4a displays the shoreline of the Ebro delta, Spain. The dotted line is the estimated reach average shoreline angle. Figure

5-4b shows an example wave climate. The wave energy contribution to alongshore sediment flux ($H_s^{12/5}T_p^{1/5}$) is energy-averaged and is corrected to a yearly distribution of waves from all directions. E.g. wave directions from "behind" the shore are not included in the cumulative distribution. Instead, the energy in those waves is subtracted from the total energy, obtaining a fair estimate for the period of concern.

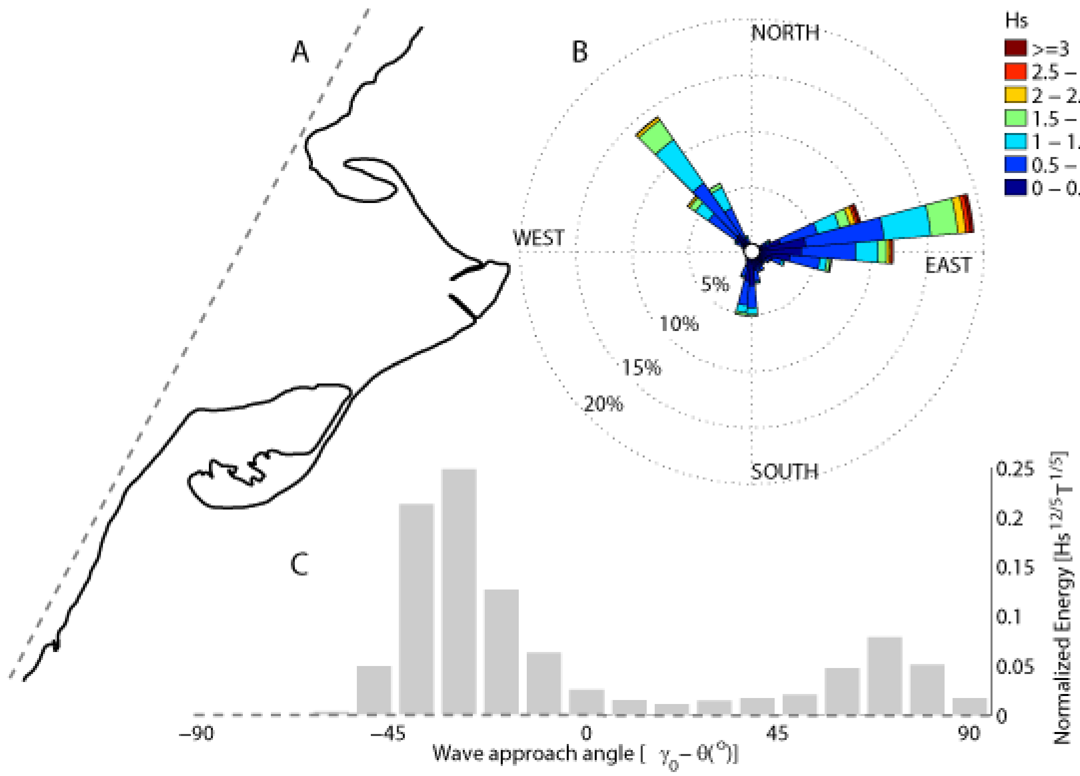

Figure 5-4: (A) The Ebro Delta. The dotted line represents the reference shoreline. (B) The energy averaged wave climate near the Ebro mouth. Source: Bolanos et al. [2009] (C) The extracted probability density function of the incoming waves as used in the model.

Two parameters determine the effect of wave directionality on shoreline evolution: wave asymmetry and diffusion. Asymmetry is defined as the fraction of wave energy coming from the left. For any shoreline, this determines the direction of the littoral transport. Diffusion (Ψ), the angle dependent term of the diffusion coefficient, determines the rate (in m^2s^{-1}) with which shoreline perturbations decay or grow.

Since a wave climate generally consists of more than one wave, individual contributions to the diffusion can be grouped together into a normalized dimensionless parameter Γ [*Ashton and Murray*, 2006a] (5). For all waves (1 through n), the diffusion coefficient (Ψ) times the occurrence determines whether Γ is positive (stable shoreline) or negative (unstable shoreline).

$$\Gamma = \frac{\sum_{i=1}^{n} \psi \Delta t_i}{\sum_{i=1}^{n} |\psi| \Delta t_i} \tag{6}$$

For an array of wave approach angles (a wave climate, Figure 5-4c), Figure 5-5b plots Γ and Q_s. For instance, a section of the southern spit of the Ebro delta (Figure 5-4a) has a shoreline orientation of -45^0. Looking at -45^0 in Figure 5-5 shows that this section of the shore is unstable ($\Gamma<0$) and that littoral transport is directed to the right (southwest is this case).

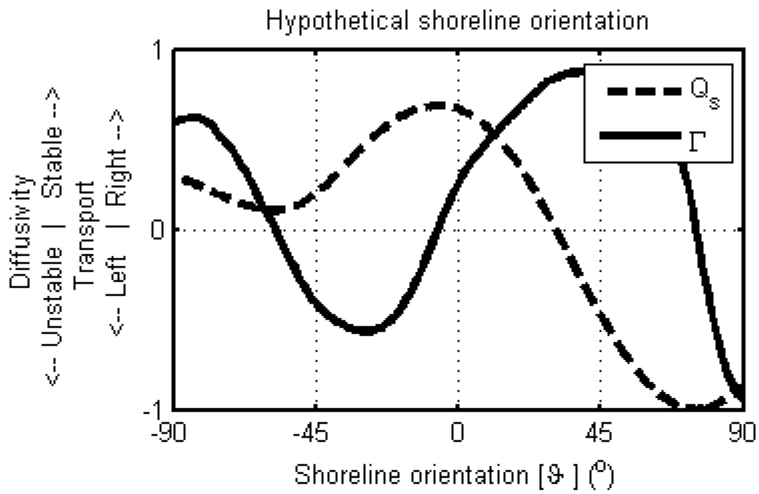

Figure 5-5: Transport and diffusivity for different shoreline orientations, with the wave climate from Figure 5-4c. Note that shadowing of shorelines to (a portion of) the incoming waves drastically changes the transport and diffusivity.

Next to using actual wave climate, we can look at wave climate effects on deltas by developing artificial wave climates. This is no trivial task, since there are infinite degrees of freedom. Two parameters create a subset of wave climates that span a broad range in physical properties [*Ashton and Murray*, 2006b]. Such a wave climate consists of four bins that span between φ_0 -90^0 and $+90^0$. Figure 5-6 shows three example wave climates based on this approach. "A" is the fraction of waves in the two left bins (waves approaching from between -90° and 0°). "U" is the fraction of waves in the leftmost and rightmost bin.

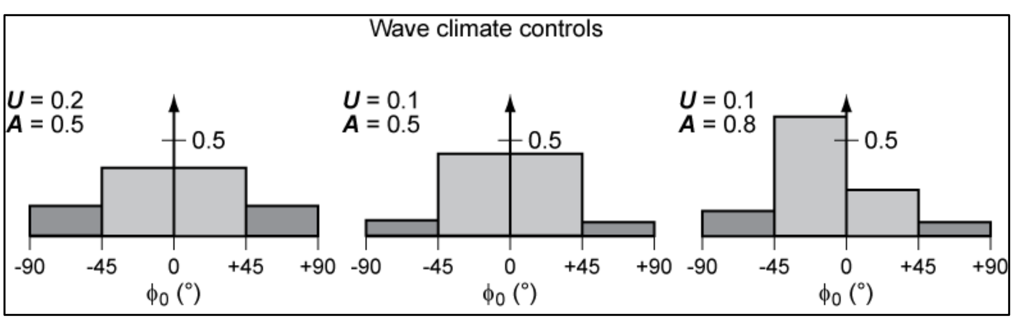

Figure 5-6: Three example wave climates using A and U.

The Asymmetry parameter corresponds directly to the asymmetry already defined for actual wave climates, because Qs is symmetric around zero. Γ is equal to 2(0.5-

U). Note that the conversion of these parameters is one-way, i.e. shoreline evolution based on an actual wave climate can usually not be adequately simulated using only A and U.

The morphological wave angle is the wave angle at the median of the normalized wave energy distribution.[2] Instantaneous littoral transport arising from a unimodal wave climate can generally be averaged at this angle, such that $\varphi_0 - \vartheta < 0$ transports sediment to the right. Because wave climates used in this report are stable for a straight shoreline, one can assume an unstable shoreline at morphological wave angles for which $\Psi < 0$.

5.3 Output

This section explains the method used to describe model results. Figure 5-7 sketches an example delta. The distance to the reference shoreline gives the river mouth shoreline displacement (and the maximum in this case). Updrift and downdrift delta parts are defined based on the asymmetry of the wave climate. The width of the delta is the distance between the first and the last displacement larger than some amount. Other properties are derived from these metrics. For instance, average upstream and downstream shoreline angles are calculated based upon the updrift or downdrift width and the river mouth displacement.[3]

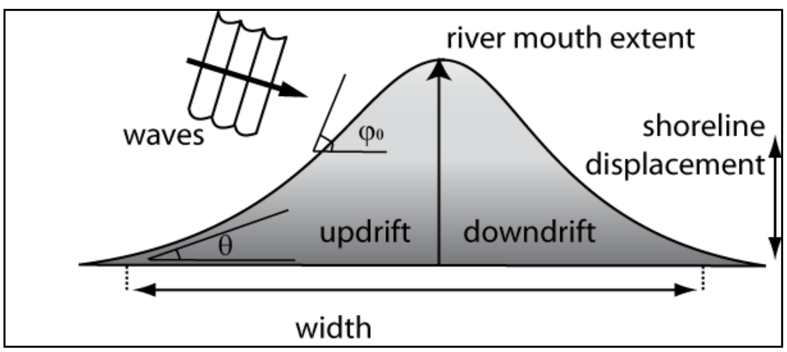

Figure 5-7: Basic delta properties

When a flying spit collapses onto the shoreline and encloses a body of water a "lagoon" forms. The reference shoreline can erode and form a "minimum shoreline displacement".

---

[2] Angle α such that $\int_{-90}^{\alpha} WaveEnergy(x)\,dx = \frac{1}{2}$

[3] Such that the shoreline angle between the River Mouth (RM) and a downdrift location W: $\tan(\alpha) = \frac{Y_{RM}-Y_W}{X_{RM}-X_W}$

5.4 Previous model results

The numerical model has been used in earlier studies (2001 [*Ashton and Murray*, 2006a; *Ashton and Giosan*, 2011; *Ashton et al.*, 2001]. The original aim was to explore the large-scale features that arise from high-angle wave instability. Innovations on earlier models are the cellular aspect, which allows the simulations of complex 2-dimensional (plan-view) features. Also, older models assumed constant (breaking) wave heights along an undulating shoreline. Deepwater, high-angle waves generate an anti-diffusive feedback between shoreline migration and the wavefield. This feedback is driven by alongshore gradients in the breaking waveheight, due to spreading and focusing of wave energy [*Falques et al.*, 2011].

Shorelines become unstable when high angle waves dominate the sediment transport. Dependent on the wave climate, cuspate features, migrating sand waves or flying spits form [*Ashton and Murray*, 2006b]. These features are dynamic even with stable environmental conditions, e.g. variations in fluvial sediment supply. Downdrift shorelines of deltas are also prone to these instabilities [*Ashton and Giosan*, 2007]. Asymmetry in the wave climate creates migrating features.

6 Deltaic response to fluvial input elimination

Here, we study the morphological development of a deltaic shoreline after elimination of fluvial sediment supply. This decrease can be the result of river engineering works, for example: river damming, or delta lobe avulsion.

How does the wave climate set the lobe abandonment regime? This section describes the reworking of deltaic shorelines due to waves, most applicable to deltas where waves are the dominant (re)shaping mechanism.

6.1 Method

We simulated the effect of lobe abandonment on deltas. Model runs are performed using different fluvial inputs and wave climates. Simulations resemble 1000 years of evolution, during which the first 500 years a delta develops. After this period, elimination of sediment input results in reworking of the lobe. These orders of magnitude are realistic, and variations herein tend not to affect the described trends [*Roberts*, 1997]. Wave climates are simulated using an asymmetry fraction and a proportion of unstable waves.

Two factors are important in lobe abandonment: (i) the shape of the delta at the time of abandonment and (ii) the wave climate. Here, we force (i) to be a morphology generated by a combination of (ii) and of varying magnitudes of fluvial bed load. We do not create arbitrary delta shapes because of the focus on physical problems.

The wave energy flux is left unchanged between all simulations, with a significant wave height and period of 1m and 5s.

6.2 Results

A decrease in riverine sediment input will disrupt a previously attained shape. The direction of littoral transport is determined by the prevalent wave approach angle. Asymmetry in this climate acts as a first order control on the delta, causing increasing differences in updrift and downdrift morphologies. Lobe abandonment ultimately results in diffusion of both updrift and downdrift shores. However, the features that occur are dependent on wave climate and on the shape of the delta prior to abandonment. This in turn determines the resulting morphology.

6.2.1 Updrift morphodynamics

During the prograding phase of the delta, the shoreline angle increases. This increase usually turns the direction of littoral transport. Delta abandonment reverses this trend. Starting at the river mouth, an increasing amount of updrift sediment is transported downdrift. Because $U < 0.5$, higher asymmetry will increase the sediment transport across the river mouth.

6.2.2 Downdrift morphodynamics

Downdrift sediment transport can induce or increase existing discontinuities in the shoreline. These discontinuities arise from the high wave approach angle at a limited section of the shoreline [*Ashton and Giosan*, 2011].

Abandonment can result into four remarkably different morphologies. Figure 6-1 shows examples of these modes. The mechanics involved in the evolution of these features is discussed in the next section.

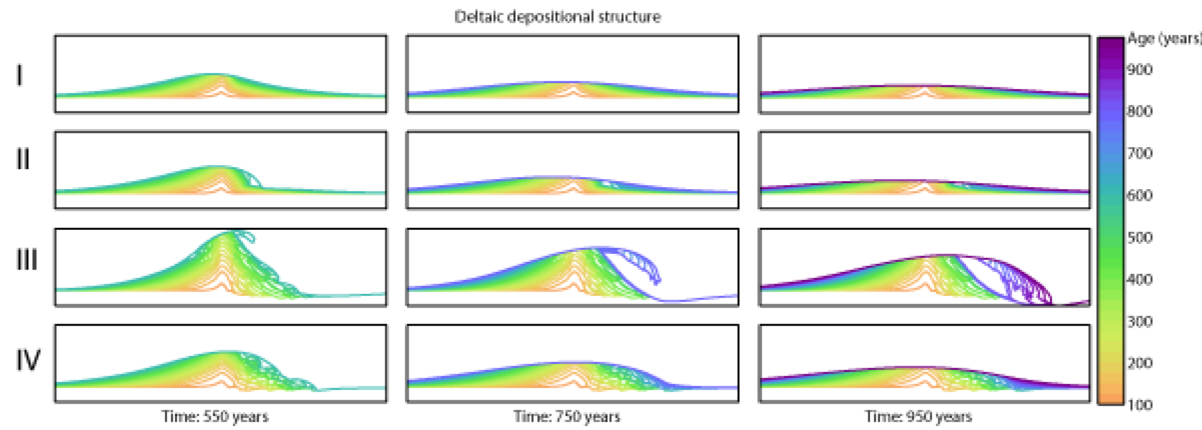

Figure 6-1: Four different modes of lobe abandonment. The colors indicate the time of deposition. Lobe abandonment occurred after 500 years of growth. I: Diffusive, II: Discontinuity, III: Spit, IV: Sandwave mode characterization.

The different modes can be characterized (ex-post) and recognized (ex-ante). This section describes the morphological development after lobe abandonment.

6.2.2.1 Diffusive Mode (I)

Low angle waves and relatively low fluvial sediment supply creates abandonment that can be characterized as a diffusion process. Because the shoreline is stable, a nonlinear diffusion equation (the diffusivity depends on the wave angle) determines the erosion. The flat cuspate/concave shape causes marine reworking to be focused around the river mouth, where alongshore transport is largest. Figure 6-2 shows the abandonment of the delta at 4 stages. Note the continuous decrease in erosion moving away from the river mouth.

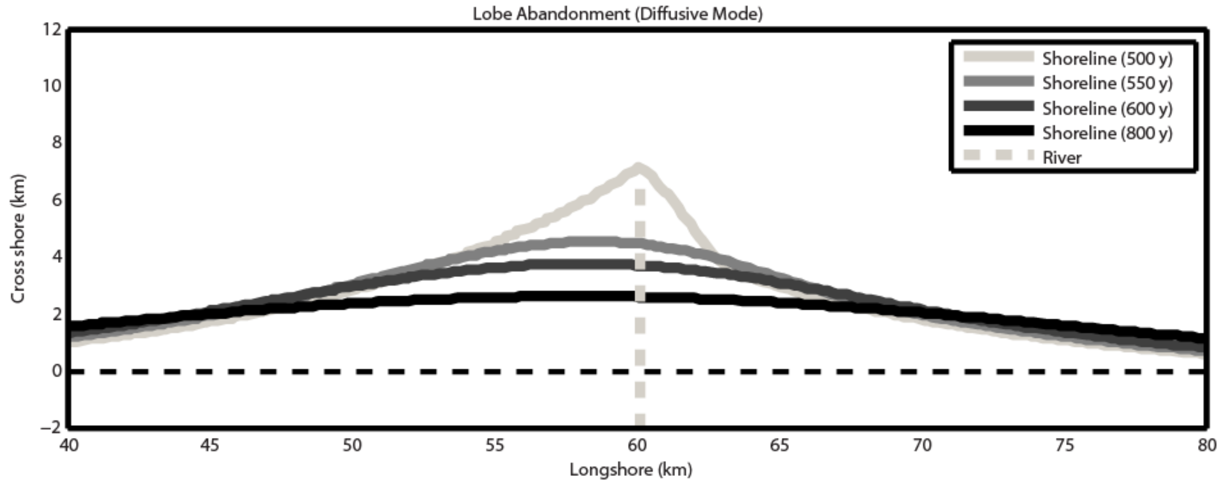

Figure 6-2: Four shoreline positions after a diffusive abandonment.

6.2.2.2 Discontinuous Mode (II)

Figure 6-3 shows the abandonment process that creates a downdrift discontinuity. Reworking of the delta extends a discontinuity in the downdrift shoreline. This initial discontinuity arises when a portion of the delta has grown beyond the angle of maximum sediment transport. The instable part forms a convex shape, while a stable shoreline further downdrift maintains a concave shoreline. At the intersection, an equal amount of littoral transport requires a discontinuity in shoreline angle.

Delta abandonment increases the shoreline angle while eroding the section downdrift of the discontinuity. As the high angle shore section decreases in size, the area eventually fills up, resulting in a process similar to the first mode. Note that the erosion occurs on the deltaic deposition. This lobe abandonment mode does not erode parts of the reference $_{y=0}$ shoreline.

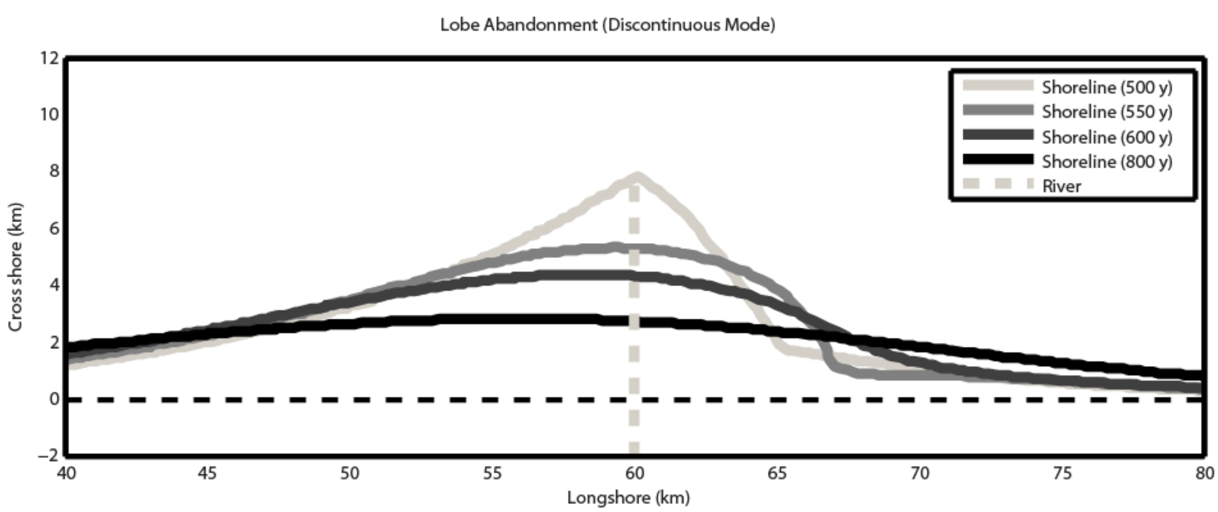

Figure 6-3: Four shoreline positions after Discontinuous Mode abandonment.

6.2.2.3 Spit Mode (III)

Similar to the discontinuous mode, a portion of the downdrift shoreline experiences high angle waves. In this case however, the length of this section is long enough for the discontinuity to translate into a spit. This spit migrates downdrift, eroding the shoreline. Orientation of the spit determines the lifetime and the amount and location of downdrift erosion. Figure 6-4 shows these four stages of lobe abandonment.

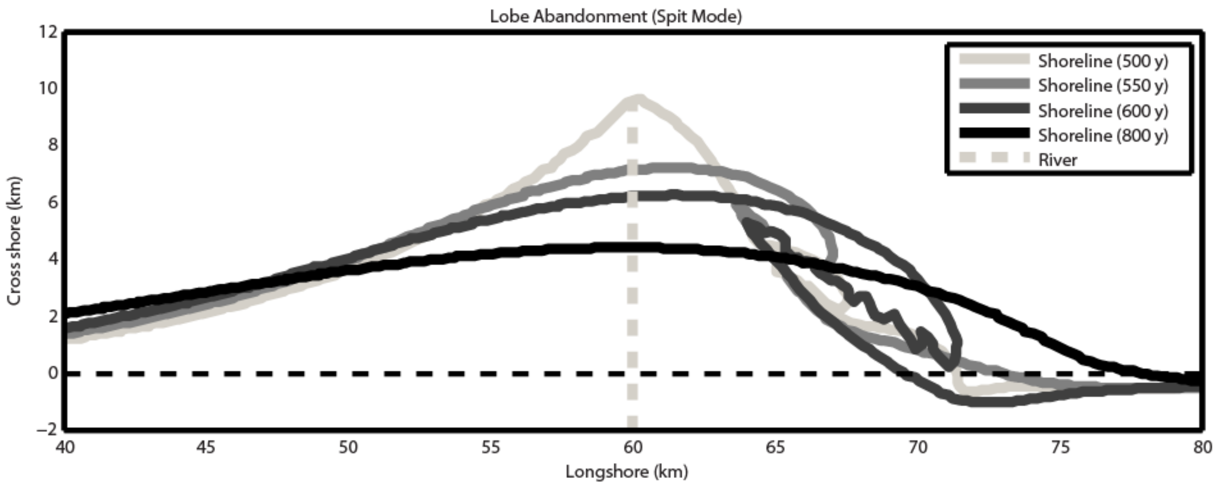

Figure 6-4: Four shoreline positions after spit abandonment.

6.2.2.4 Sand Wave Mode (IV)

Trains of sand waves characterize a highly unstable shoreline. These sand waves increase the littoral transport away from the delta. In addition, this instability creates lagoons that increase the total area of the delta. These two effects limit the steepness, decreasing the magnitude and lifetime of the spit after the lobe abandonment. Figure 6-5 shows the deltaic shoreline at four stages in the abandonment process.

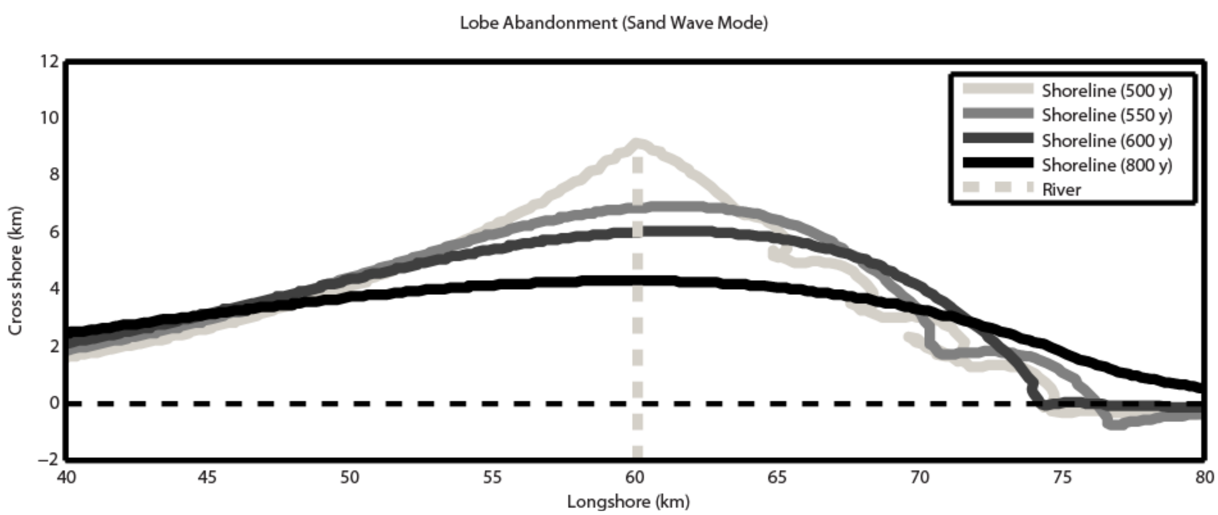

Figure 6-5: Four shoreline positions after sand wave abandonment.

6.2.3 Mode recognition

As hinted upon earlier, the formation of downdrift coastal features depends on both wave climate and pre-abandonment delta shape. These controls together determine the shoreline stability and direction of its evolution. The downdrift shoreline angle in particular controls the morphodynamics of the marine reworking.

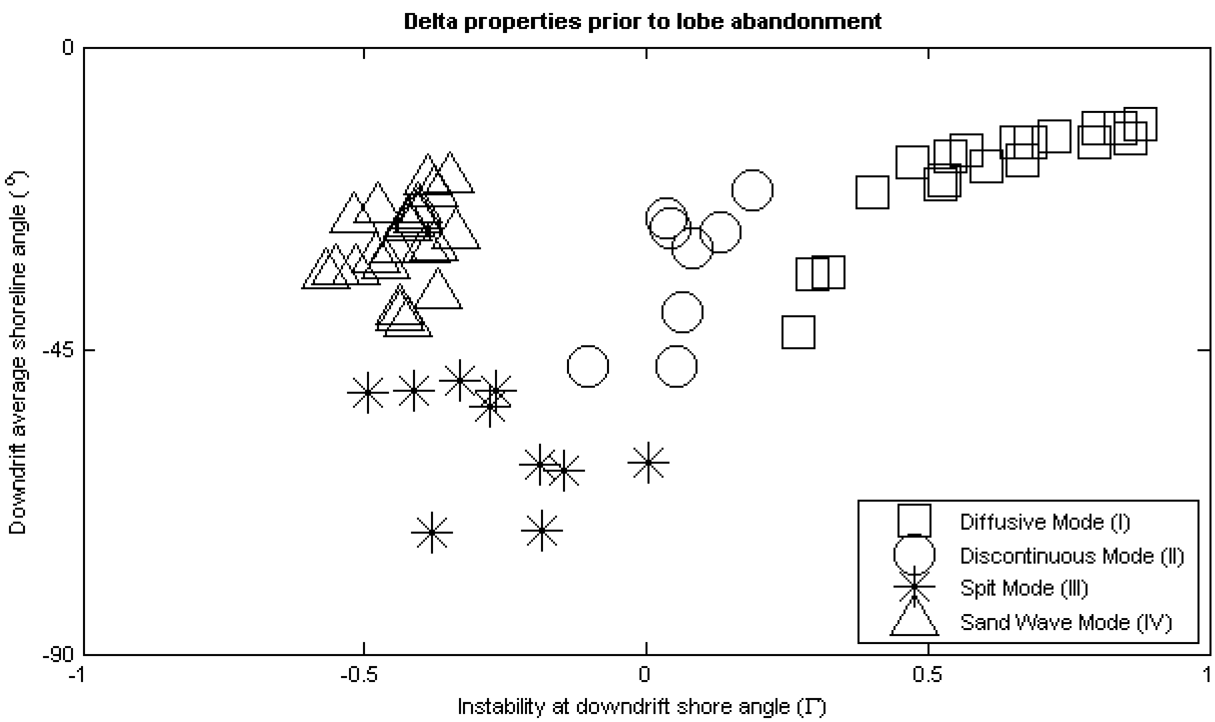

Figure 6-6: Ex-ante lobe abandonment recognition. Four modes are plotted against downdrift wave climate and downdrift shoreline angle. NB: These are dependent variables.

Figure 6-6 shows the occurrence of lobe abandonment modes related to the downdrift shoreline instability and the downdrift shoreline angle. Except for the external spit, shoreline instability alone separates lobe abandonment modes. External spits arise when not just the shoreline angle is unstable, but also when this instability has not fully developed into the flattening of the downdrift shoreline.

The downdrift shoreline angle develops as a result of the wave climate and the fluvial input. Higher fluvial dominance[4] generates greater shoreline angles. Wave climate asymmetry up to about 0.75 initially also decreases the transport updrift and downdrift. However, as the asymmetry increases, the unstable downdrift shoreline lengthens, effectively increasing sediment transport downdrift and flattening the shoreline angle. The change in the aspect ratio causes lobe abandonment spits to collapse relatively quickly. The amount of asymmetry where the second factor outweighs the first is dependent on the fluvial dominance ratio.

[4] A ratio of the fluvial bedload with symmetric deltaic shoreline diffusivity:

$$\frac{Q_r}{Q_{s,updrift}+Q_{s,downdrift}}=\frac{Q_r}{\rho_s \cdot H_s^{12/5} \cdot T_p^{1/5} \cdot K_2 \cdot \left(1-\frac{3}{2}U\right)\cdot \frac{5}{11}}$$

Figure 6-7 shows the downdrift shoreline angle resulting from several environmental controls.

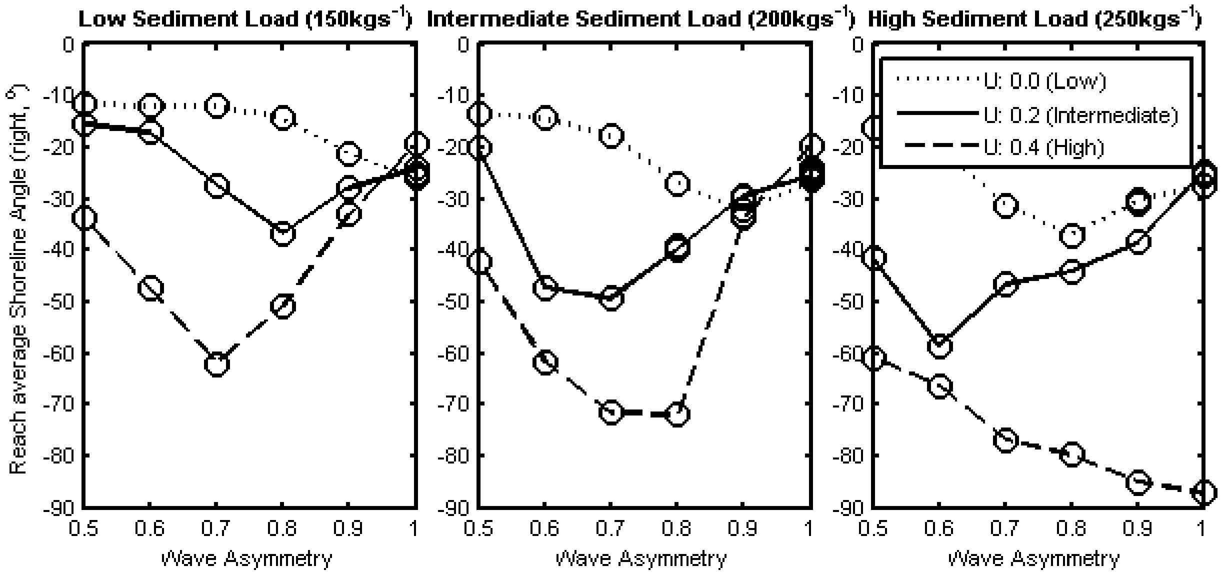

Figure 6-7: Wave climate control on the downdrift shoreline angle.

6.3 Discussion

Effects of lobe reworking are not confined within the original extent of the delta. Erosion of the (non-deltaic) shoreline occurs when an asymmetrical wave climate creates a spit that migrates away from the river mouth. Erosion is due to the positive gradient in sediment flux between the shadowed and non-shadowed portion of the shoreline.

Transport of sediment across the river mouth, in combination with an eroding downdrift delta, result in a river mouth groyne effect [*Giosan*, 2007]. This groyne effect results in the formation of barriers that can develop into spits, especially in case of retreating river mouths.

A quick glance at modern delta stratigraphy shows that lobe reworking modes can be distinguished. The Ebro delta, Spain, is perhaps a trivial example of where reworking of lobes has caused the growth of external spits [*Canicio and Ibanez*, 1999]. There is also lobe reworking at the Rhone delta, France [*Vella et al.*, 2005]. This is signaling the growth of an internal and an external spit. Diffusive reworking seems to take place at the Ombrone River, Italy [*Pranzini*, 2001].

6.4 Conclusion

Four distinct morphodynamic and morphologic scenarios can develop after delta lobe abandonment: diffusive mode (I), discontinuous mode (II), spit mode (III) and sandwave mode (IV). Stable updrift and downdrift shorelines characterize the diffusive mode. The abandonment process follows that of an ordinary diffusion equation (eq. 4). There is gradual increase in deposition of deltaic sediments away from the river mouth. The second mode (II) arises when a discontinuity in the downdrift shoreline increases due to increased transport of sediment downdrift. Shadowing erodes parts of the downdrift delta. Infilling of these sections by younger sediments occurs, but it does not result in the formation of a lagoon. When a larger section of the downdrift shore is unstable, a spit (III) grows that migrates away from the old river mouth. Larger downdrift shoreline angles cause spits to shadow and erode deltaic and non-deltaic sediments. An increasing asymmetry in the wave climate promotes flattening of the delta. These sand waves (IV) cause spits to collapse onto the delta.

The wave climate sets the abandonment regime by controlling the downdrift shoreline evolution via the shape of the delta and the local wave climate.

The next chapter will analyze the lobe abandonment that occurred at the Ebro delta, Spain.

7 Case study: Ebro Delta

Two Late Holocene river avulsions have shaped the current Ebro Delta, Spain. Subsequent abandonment of two old lobes created spits. Modeling can quantitatively constrain development hypotheses, i.e. what are fluvial and marine limits for this particular evolution? How is lobe abandonment embedded into Ebro delta morphology? The model results presented here show the environmental requirements needed for the development of the characteristic spits north and south of the current river mouth. These spits constrain spatial and temporal aspects of the Ebro's evolution.

Results are organized the following way; first an overview is given of the Ebro delta. Section 7.2 explains the particular model parameters used. Results of the simulations and of the spit shapes are in section 7.3. This chapter ends with a discussion and a conclusion.

7.1 Ebro Delta

Situated on the Mediterranean Sea, the Ebro delta displays a very distinctive shape, see Figure 6-1. This shape is commonly attributed to the reworking of two historic lobes, on either side of the present river mouth. Figure 7-2 sketches 4 stages in the development.

Figure 7-1: The current Ebro Delta, Spain [*NASA*, 2000]. The spit to the south is called "La Banya". The spit to the north is the El Fangar Spit. The Ebro River extends about 25km into the Mediterranean.

Radiocarbon dating shows Ebro delta existence from about 6000 years BP, when Holocene sea level rise stabilized [*Canicio and Ibanez*, 1999]. Although different opinions exist about the timing of the first lobe, [*Canicio and Ibanez*, 1999] state that a relatively small cuspate wave dominated delta was present 3000 years BP. Around 1500 years BP (the early Middle Ages), progradation rates 2-3 times faster than before formed a fluvial dominated delta, extending around 25 kilometers into the Mediterranean. Upstream avulsion created a new lobe, oriented to the north. This lobe was active up until 300 years BP, when a new avulsion formed the present river mouth. Different progradation rates have their origin in fluvial sediment supply, commonly ascribed to land use changes and subsequent alluviation during the Middle Ages [*Thorndycraft and Benito*, 2006]. River damming and irrigation are responsible for the current coastal retreat [*Sanchez-Arcilla et al.*, 1996].

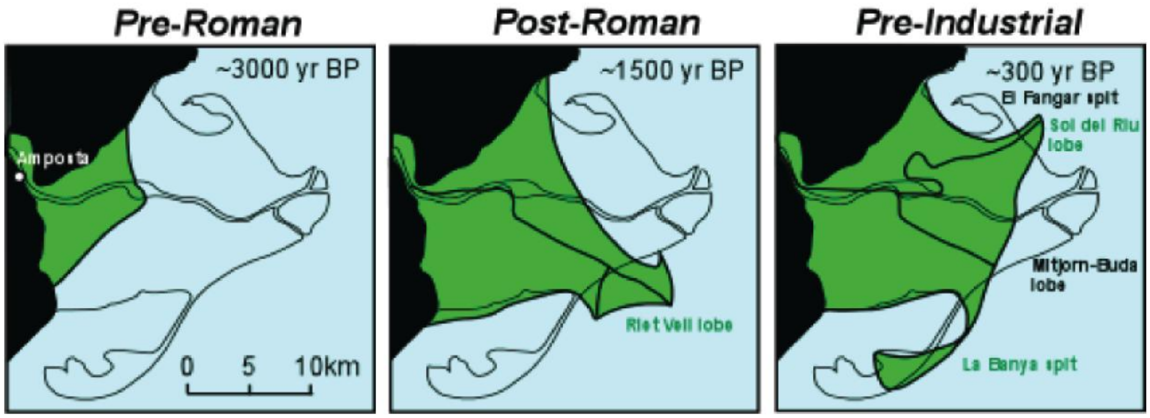

Figure 7-2: Conceptual evolution. Copied from [*Ashton et al.*, 2010], modified after [*Canicio and Ibanez*, 1999].

Many studies have looked into the Ebro Delta morphodynamics on the short-term [*Jimenez and Sanchez-Arcilla*, 1993; *Jimenez et al.*, 1997; *Sanchez-Arcilla et al.*, 1998] and on long-term morphology [*Canicio and Ibanez*, 1999; *Ibanez et al.*, 1997]. However, no quantitative study exists that looks into century scale deltaic change.

7.2 Method

We modeled the building and reworking of individual lobes. Each lobe builds at set angle with respect to the shoreline. This indirectly determines the characteristics of the wave climate as it reworks the delta. After 15 kilometers, the fluvial input is either terminated or builds out a delta at a different angle. This length is chosen to reflect the channel growth at the period of rapid progradation.

The wave climate is extracted from a buoy located near the river mouth at a water depth of 60m [*Bolanos et al.*, 2009]. Other sources (hindcast meteorological wave models) are available [*Cavaleri*, 2005; *Jimenez et al.*, 1997; *Ratsimandresy and Sotillo*, 2003], having similar characteristics. The buoy data is located closest to the delta. The wave climate data is refracted based on parallel depth contours up to a depth of 15m. Significant wave height is 0.7 meters; the wave period is 4.3 seconds.

A small adaptation in the model accounts for the rocky (non-deltaic) coast north and south of the Ebro delta, such that the initial shoreline is non-erodible.[5] The littoral transport function used in the model is calibrated using recent shoreline measurements [*Jimenez and Sanchez-Arcilla*, 1993]. For the duration of an active delta lobe, the sediment input is set at $65 kgs^{-1}$, an approximation of historical fluvial supply [*Vericat and Batalla*, 2006]. Nearshore bathymetry used in the model is retrieved from Guillen and Jimenez [1995] and Jimenez and Sanchez-Arcilla [1993].

[5] This rocky coast is modeled by disabling transport out of a cell which is on the initial shoreline.

7.3 Results

Different stages in the delta evolution are plotted in Figure 7-3. The first lobe builds at 5°, until it reaches 15km in length. This happens after about 500 years. A spit grows, while the second lobe progrades at -30°. At 900 years, a second avulsion starts the third lobe.

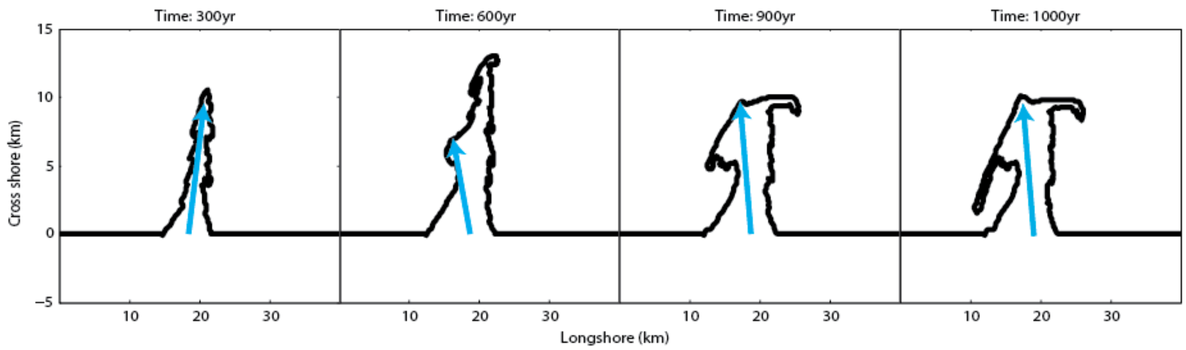

Figure 7-3: An example simulation showing the formation of two spits after avulsions. Blue arrows indicate river positions at selected periods.

7.3.1 Individual lobes

Simulations show that spits develop after abandonment of individual lobes. These lobes build at various angles with respect to the shoreline, advancing too fast for the waves to rework it into a cuspate shape. Figure 7-4 shows these individual lobes within the lobe abandonment framework.

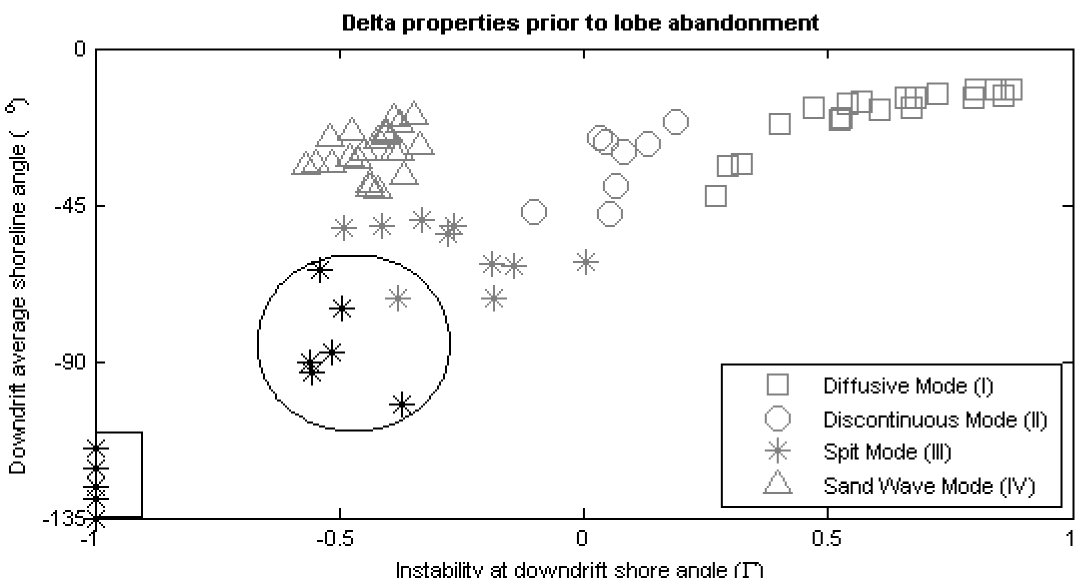

Figure 7-4: Downdrift shoreline parameters in the Lobe Abandonment framework. Markers in the circle (square) have a downdrift angle to the right (left). The downdrift angle is corrected for changes in abandonment direction (within the same reference, these angles are ± +120^{0}).

7.3.2 Spit characteristics

One interesting remark is the spit shape evolution. As the shoreline retreats, it transports the sediment based on its local shoreline orientation. A spit grows if a portion with sufficient length is highly unstable with respect to the wave climate. Figure 7-5 shows two example spits, along with several characterizing parameters.

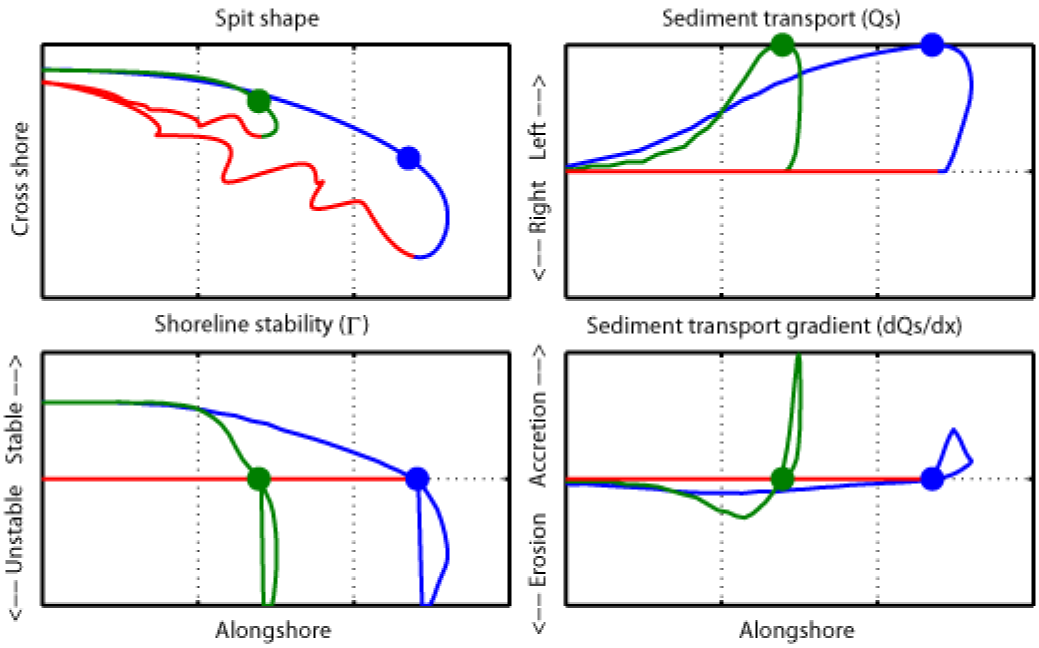

Figure 7-5: Example spits. The dot represents the location of maximum alongshore transport. NB: these spits are shown for the sole purpose of explaining the effect of spit curvature on their rate of growth.

Somewhere along the tip of the spit, the wave climate passes the angle of maximum transport. At this location, where $\Gamma = 0$, there is a shift from erosion to accretion. The magnitude of shoreline change is only dependent on the local shoreline gradient. Other processes left unchanged, the spit curves along its tip, increasing its width [*Ashton et al.*, 2007]. The amount of curvature controls the magnitude of the erosion and vice versa. These two processes are in dynamic equilibrium. Compare the "green" and "blue" spit of Figure 7-5; the higher curvature of the green spit results in greater erosion and deposition.

Assuming that the "base" of the spit retreats with a certain velocity, the angle at which the spit grows is controlled by the difference with the erosion at the tip. The latter is has its maximum at a curvature that is similar to the minimum barrier width. Fast retreating river mouths thus grow narrow (i.e. small radius at the tip) spits. Slower retreat lets spits widen. The interesting shape of the La Banya spit informs us of the possible of the two-staged growth, the first part with a fast retreating river mouth.

7.3.3 Lobe interaction

The Ebro is shaped by the interaction between different lobes. This interaction, or succession of deltaic lobe angles, eventually decreases river mouth retreat, resulting in a slower retreating spit. Figure 7-6 shows river mouth retreat rate for a lobe at 5 degrees, similar to the oldest lobe at the Ebro (now La Banya spit).

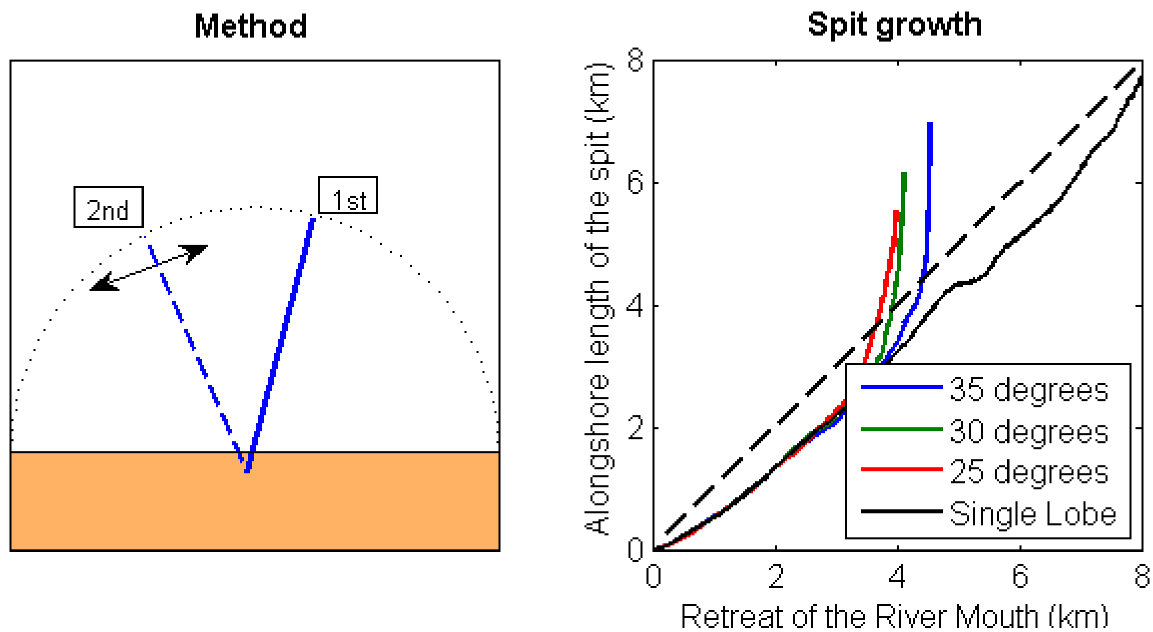

Figure 7-6: Left; sketch explaining the method. The first lobe builds out at 5 degrees. Interaction takes place when a second lobe builds out along the dotted line after abandonment of the first. Right; growth of the spit compared to retreat of the river mouth. Note that this line follows the evolution of about 750 years. The dotted line is where the retreat of the rivermouth (in km) exactly corresponds to the alongshore building of the spit. The different colors stand for the amount of interaction with the retreating lobe. E.g. 25 degrees is the different in angle between the 2nd and the 1st lobe.

Figure 7-6 should be interpreted the following way. At the time of abandonment, both river mouth retreat and spit length are 0 km. When the river mouth retreats, that speed is at first larger than the speed with which the spit grows. Halfway the curve, the spit advances with the same speed. Eventually, interaction with the new lobe (when the different colors begin to diverge from the black line), is creating the spits to curve. This curvature slows down the rate of growth of the spit, when the river mouth no longer retreats.

The relation between river mouth retreat and the onset of spit curvature shows us that the straight (barrier) section of the La Banya spit should be a good approximation of the amount of retreat of the old river mouth.

7.4 Conclusion

The Ebro morphology is shaped by the avulsion of two deltaic lobes, to the north and south of the current river mouth. Spits grow after a change in active lobe. A relatively large rate of sediment supply, and thus a relatively young delta, is a necessary condition for the development of these spits. The retreat rate of a lobe determines the progradation velocity and the curvature of spits. Modeling of the abandonment of individual lobes informs us that lobe interaction is responsible for the spits curvature.

8 Deltaic response to fluvial input variation

How does fluvial variability affect autogenic shoreline instability? Subsection 7.1 treats the method used. This chapter will analyze autogenic instability and the impact of fluvial sediment input variability.

8.1 Method

The wave climate is chosen such that the downdrift shoreline experiences predominantly high angle waves. Larger asymmetry (A) and a higher proportion of unstable waves (U) lengthen the downdrift shoreline, improving the accuracy of the signal extraction. Therefore, these simulations are performed using A: 100% and U: 40%. Note that any wave climate causing downdrift shoreline instability creates quantitatively (and also qualitatively) similar results. Waveheight is 1 meter, waveperiod is 5 seconds. 1000 model years are simulated.

The statistics of sand wave migration are extracted from the model by counting all local minima and maxima in the downdrift shoreline. This analysis returns the highest frequency present in the signal. Other signal processing tools, Fourier transforms and wavelet correlation, are difficult to physically relate to this particular process.[6] Figure 8-1 shows both sand wave period and length (horizontal and vertical transects of Figure 8-3).

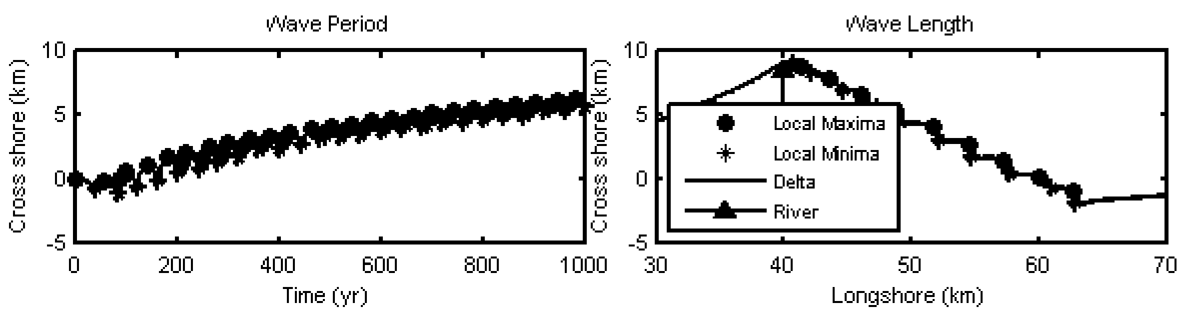

Figure 8-1: Analyzing wave period (at y=50km) and length (at t=600y). The wave length is used to calculate the sand wave celerity; diagonal lines in Figure 8-3.

8.2 Results

8.2.1 Autogenic instability

Because the wave climate is asymmetric, shoreline instability migrates downdrift from the river mouth. Sand waves and reconnecting spits extend from the slight curvature present at the convex shoreline. Figure 8-2 shows an example of a deltaic shoreline experiencing these waves.

[6] For a number of reasons, i.a. short section of sand wave field, formation of flying spits, difficulties in alongshore variations in characteristics.

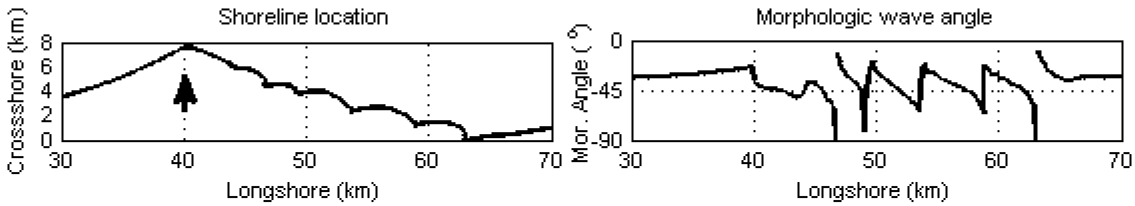

Figure 8-2: Example delta with high angle wave instability. The arrow represents the location of the river. The morphologic wave angle is a single wave approach angle such that the local morphodynamic effects equal that of the local wave climate.

The process of migrating instability can be viewed both in space (wave length, figure 1) and in time (frequency). Figure 8-3 shows the delta extent in both time and space. The gradient of the fluctuations therefore equals the sand wave celerity.

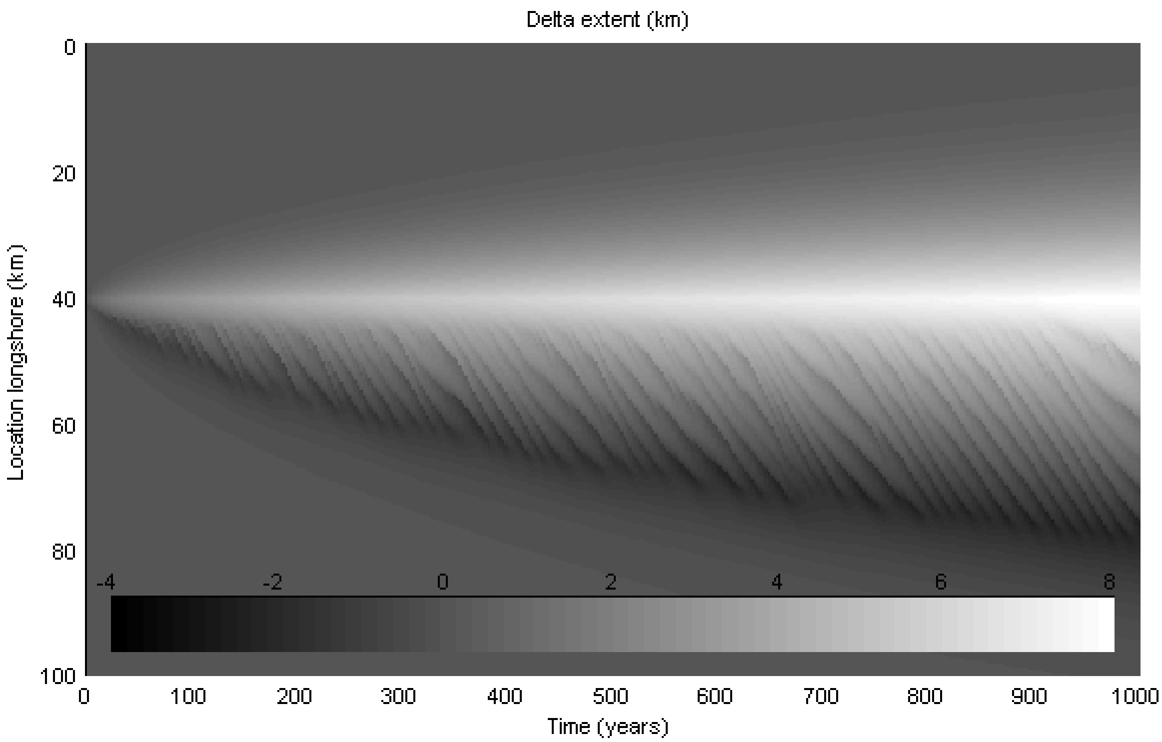

Figure 8-3: Delta development through 1000 years. The Colormap indicates the amount of (crossshore) shoreline displacement.

Using the technique described earlier, we can analyze patterns in the downdrift shoreline. Without any variation in the sediment supply, autogenic sand waves form and migrate with a period of close to 15 years. The sand wave celerity is close to 0.24 kmy^{-1}.

8.2.2 Allogenic interaction

Sand waves change when the fluvial input is forced with a certain frequency and amplitude. A decrease in riverine sediment supply changes the shoreline angles around the river mouth: updrift sediment is transported downdrift. Increasing forcing periods should increase the size of the sand waves.

Figure 8-4a plots the frequency of the instabilities compared to the initial forcing. Having high amplitude, 80% in this case, results in instabilities of equal frequency. Decreasing this amplitude results in a decrease in wave period, but only if there is accommodation space. E.g. a fluvial forcing period of 50y, significantly higher than the autogenic period, will cause autogenic sand waves to form if the forcing variability is lowered. The dotted line represents a one-to-one transfer of frequencies. Sufficiently high forcing amplitudes make sand waves approach this line.

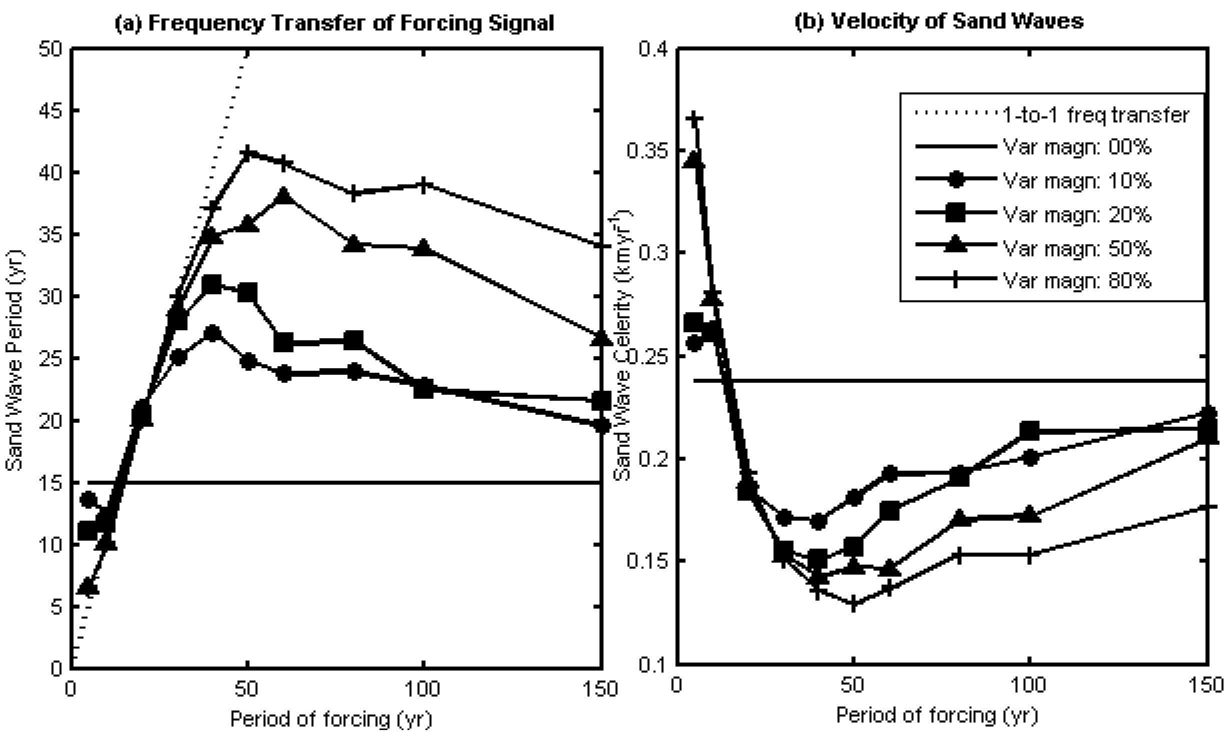

Figure 8-4: (a) Resulting wave period forcing related to fluvial forcing, (b) Resulting sand wave celerity, calculated as the frequency times the wavelength. The sediment input is 100kgs^{-1}.

Increasing periods even further beyond 50 years creates a morphodynamic pattern that is a mix of both autogenic and allogenic instabilities. There is "accommodation space" of high frequency autogenic periodicity if the system is forced with river pulses of 100 and 150 years, regardless of the amplitude. An allogenic signal still propagates at longer periods.

Figure 8-4b shows the speed of the instability, compared to the frequency and amplitude of the forcing. High frequency forcing generally creates faster propagating waves. Decreasing to lower amplitudes (to 10% of the mean fluvial input in this case) causes high and low frequency forcing to allow autogenic instability. This frequency changes along the shoreline. Figure 8-5 plots the (lowest recognized) period of sand waves versus the distance from the river mouth.

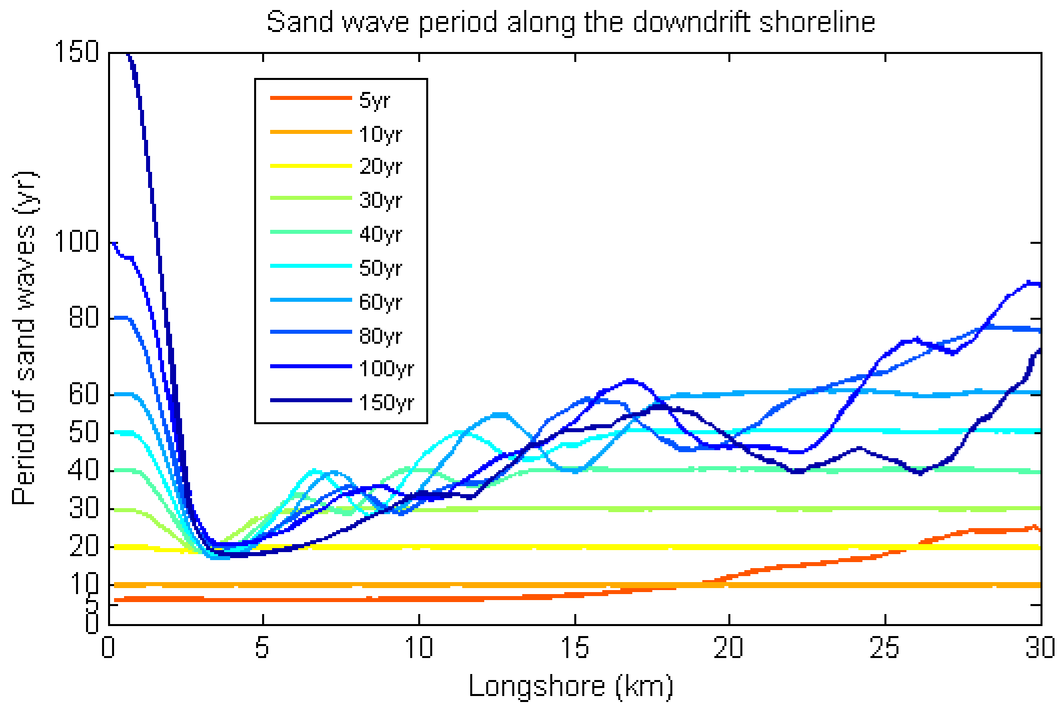

Figure 8-5: Changes in the instability along the downdrift shoreline, with high amplitude forcing.

At the river mouth the "sand wave" period equals the forcing period because there is no autogenic signal present. Further away however, sand waves form during high sediment input periods. This causes the sand wave frequency 4 km from the river mouth to be significantly higher. Because the sand wave celerity is dependent on the frequency, the signals eventually merge and self organize into one dominant period. Lower frequency signals are shredded by the autogenic variability of the downdrift shoreline.

8.3 Discussion

Although there are few natural examples of downdrift deltaic shoreline instability, there are certain findings worth mentioning. First is the influence of long-term fluvial fluctuations on sand wave formation. Second is the interaction between allogenic and autogenic emerging features. The "shredding" of the allogenic signal suggests another difficulty in finding hinterland climate records in the depositional structure.

8.4 Conclusion

The frequency of the fluvial input, with high enough amplitudes, forces an equal frequency of instability on the downdrift side of the delta, completely shredding any autogenic variability. However, small magnitude variations in the fluvial signal create accommodation space for this autogenic instability. The same holds for longer timescale fluctuations. Differences in sand wave celerity cause individual sand waves to merge into one dominant period, equal to the forcing period. Fluvial input signals carrying a higher frequency than the autogenic fluctuation slowly self organize into longer timescale sand waves.

9 Case study: Godavari Delta

How do large climate fluctuations imprint themselves onto the deltaic history? We used a simplified exploratory computer model to see the effect of temporal variability in fluvial input to the shoreline development of river deltas. We modeled the marine environment to resemble the Godavari Delta, India. This delta is chosen because of the monsoonal character of its fluvial supply, with 95% of its discharge within six months, thus being susceptible to longer-term megadroughts [*Nageswara Rao et al.*, 2010].

Section 9.1 discusses the Godavari Delta. Subsection 9.2.1 and 9.2.2 contain respectively the downdrift and updrift morphology. The discussion and conclusion are stated in section 9.3 and 9.4.

9.1 Godavari Delta

The configuration of the model is based on a simplification of the Godavari Delta. The wave climate data is extracted from the NOAA WaveWatch III model, using meteorological hind cast data between 1997 and 2011 [*NOAA*, 2011]. The wave climate is in good correspondence with the actual trends in current shoreline development as reported in Nageswara Rao et al. [2010]. Note that the magnitude of overall shoreline variability is calibrated using this same dataset.[7] Figure 9-1 plots the wave climate and shows the resulting morphologic wave approach angle on the Godavari Delta. Wave Rose bins are weighted based on their littoral transport capacity and colored based on the wave height. Average wave height and wave period are 1 meter and 8 seconds. When no other information is provided, sediment input amounts 175 kgs^{-1} [*Syvitski and Saito*, 2007].

[7] The empirical constant K_1, see chapter 4, is calibrated by comparing the measured recent shoreline change with the transport function calculations (3).

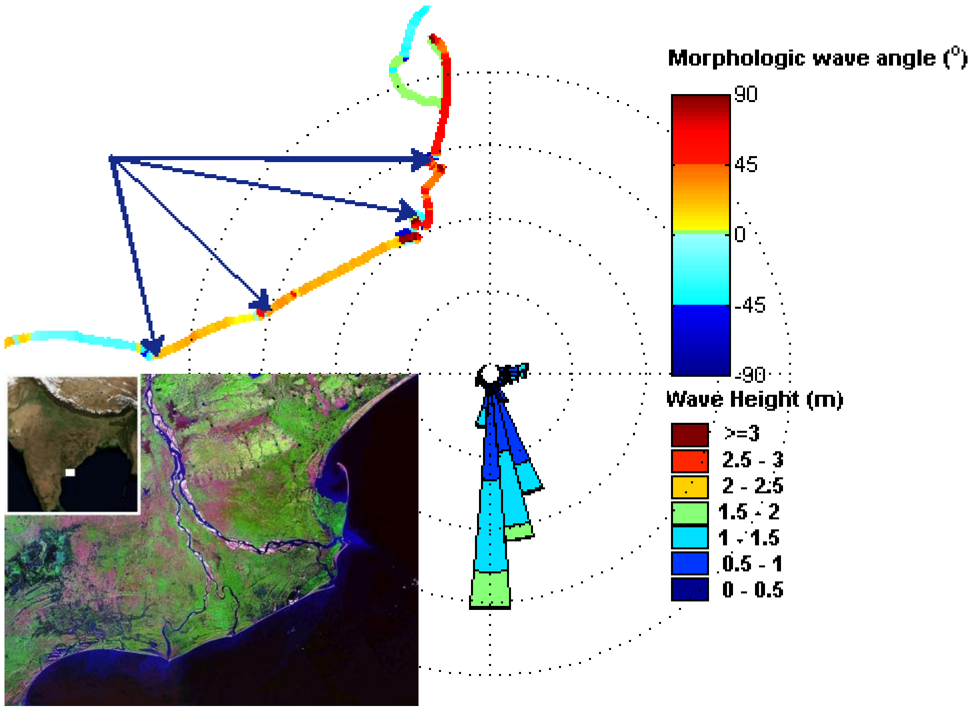

Figure 9-1: Bottom left; plan view Godavari delta, India [*NASA*, 2000]. Right; wave climate near the Godavari Delta. Notice the peak in direction from the south. The blue arrows indicate the current locations of river mouths on the shoreline.

9.2 Results

9.2.1 Downdrift deposition

This section will discuss the morphodynamics of the downdrift delta and its dependence on fluvial variability.

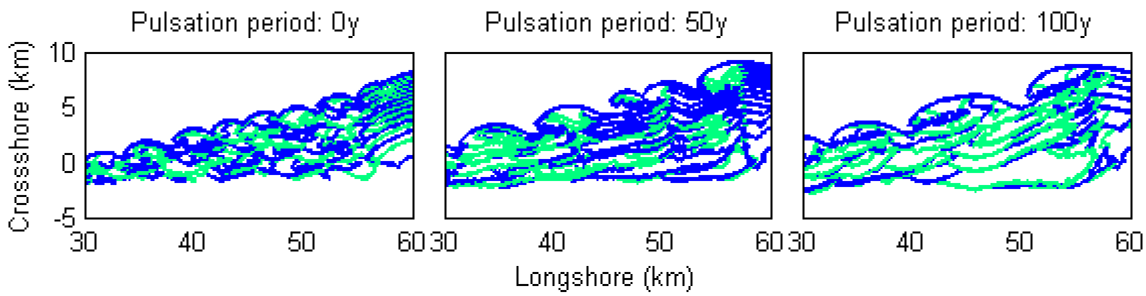

Figure 9-2: Downdrift morphology with and without fluvial variability. Every 50+50n years shows a green line, every 25 + 50n years shows a blue line. For a 50y period, this means that a blue line is the deltaic extent at the end of a 25y "dry" period. Large elongated gaps characterize lagoon formation.

As shown in Figure 9-2, an increase in fluvial variability creates a downdrift shoreline that is characterized by spits and the formation of lagoons.

Short-term morphodynamics can explain this difference in morphology. As the sediment load determines the shape of the delta, periods of high sediment load (Q_H) result in the buildup of a more pronounced cuspate shape than periods of low sediment load (Q_L). The transition from Q_H to Q_L causes the rate of longshore transport to be greater than the riverine input.

Dependent on the relative magnitude of the change, a reworking of the active lobe takes place. Sediment is transported in the net transport direction, north in this case. A spit forms on the downdrift side of the lobe in cases where the maximum downdrift shoreline orientation with respect to the incoming waves is strictly larger than the angle of maximum transport. As the tip of the spit reconnects to the shoreline, a lagoon is formed in the encapsulated region. Figure 9-3 shows the deltaic shoreline before, during and after the decrease in sediment input.

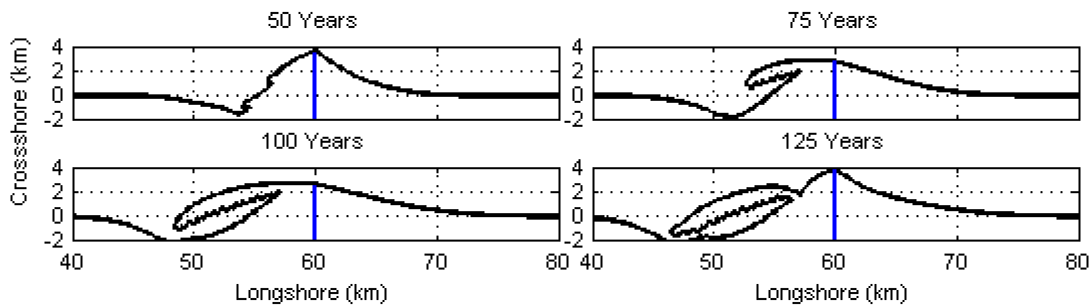

Figure 9-3: The blue lines indicate the position of the river. Between year 50 and year 100, the sediment input is decreased.

Higher sediment loads creates larger downdrift shoreline angles and increases the "erodible mass" of the delta.[8] Amplitude and period of the fluvial input control therefore the magnitude and lifetime of this spit. The latter because the formation is forced one-to-one with the forcing period. Amplitude and sediment load control the area of downdrift lagoons. In addition, the spits cause erosion due to wave shadowing. Figure 9-4 plots the total lagoon area and the maximum erosion caused by wave shadowing after 900 years.

[8] This mass can be conceptualized as the difference in the dynamic equilibria of the delta between both fluvial supply rates.

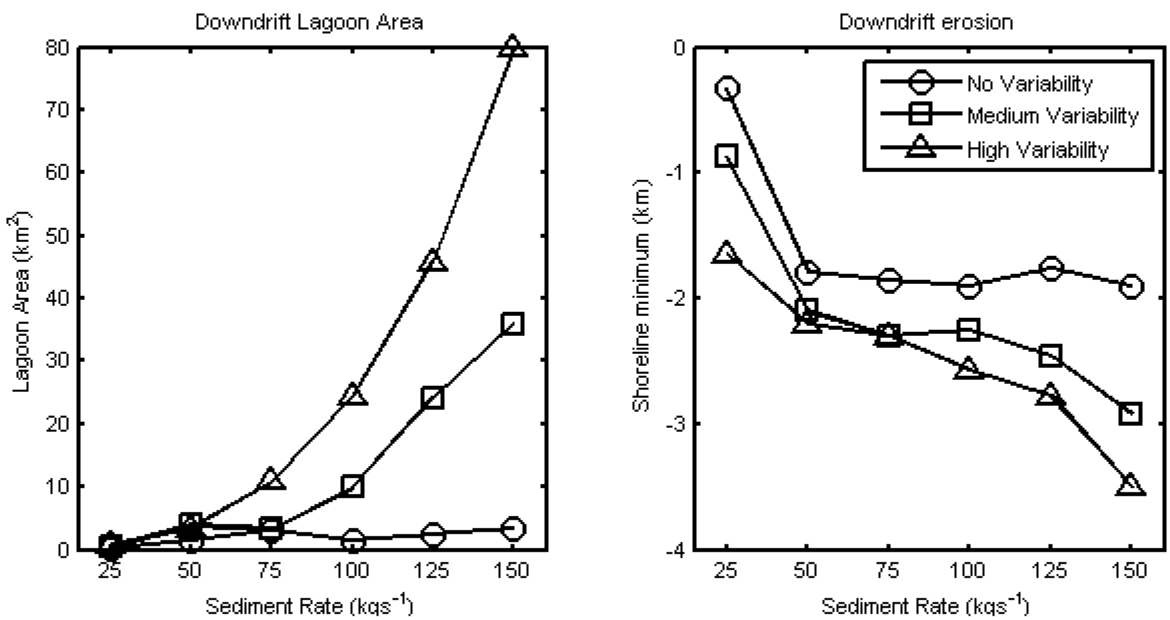

Figure 9-4: Increase in lagoon size and erosion due to fluvial variability and sediment rate.

9.2.2 Updrift deposition

Also the updrift depositional pattern is dependent on the amplitude and frequency of the fluvial input. Constant sediment load gradually layers deposits on the updrift side, independent of the global trend in littoral transport. Periods of low sediment input cause the delta to have a different equilibrium shoreline orientation. Figure 9-5 shows the updrift deposition resulting from different periods of pulsation. Erosion of the delta close to the river mouth creates clear transitions in deposition age. In addition, deposits with fluvial variability develop convex beach ridges close to the river mouth. Further away from the river mouth, the variability does no longer effect the deposition.

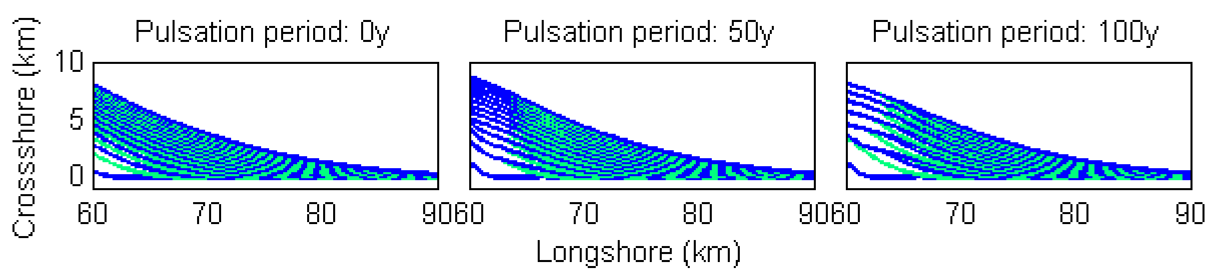

Figure 9-5: Updrift delta composition of cases with different forcing frequencies.

9.3 Discussion

Comparison of the modeled deltaic shapes and the Godavari Delta falls short on more than one occasion. However, in contrast with earlier suggestions, The development of the prominent spit on the north side of the Godavari could arise due to an decrease in fluvial sedimentation, note that this is different from Nageswara Rao et al. [2005]. In this wave climate, a decrease in input would create a spit. Note that the reported origin of the prominent Kakinada spit coincides with a series of monsoon failures known as the Victorian drought [*Nageswara Rao et al.*, 2010] [*Cook et al.*, 2010].

In addition, deposition updrift translates more or less linear with climate signals. The dynamics of an unstable shoreline make the same translation downdrift very difficult.

9.4 Conclusion

River delta development and morphology is dependent on long-term variation in sediment supply. Regular erosion updrift leaves a sedimentary pattern that is arcuate around the river mouth, while the shoreline shape of the delta is predominantly cuspate. Longer period and larger magnitude of fluctuations increase the extent of this erosion.

Decreasing sediment delivery causes spits to form on the downdrift side of the delta, when the shoreline orientation is strictly larger than that where maximum sediment transport occurs. These spits eventually collapse and form a lagoon on the downdrift side of the delta. The size and location of the lagoons and the shape of the depositional pattern depends on the magnitude and the period of fluvial oscillations.

10 Discussion & Conclusion

There are a variety of deltaic responses to fluvial delivery variability. This report focused on (i) fluvial input elimination and (ii) fluvial input variation in a wave-dominated setting. River damming or lobe abandonment can create a permanent discontinuation in sediment input. Time-periodic input can be the result of climate fluctuations.

Features modeled and shown in the last four chapters all arise from one feedback inherent in alongshore littoral transport. This simple model provided quantification of river bedload vs. wave energy. Straightforward changes in sediment delivery showed that broad categorization is possible. Other natural processes can and will change the frameworks and other findings presented here.

(i) There are four distinct modes in which lobe abandonment can take place. The shoreline shape and wave climate determine how littoral transport reworks the plan-view delta. Going from high to low downdrift instability, abandonment can be characterized by the following modes: diffusive, discontinuity, a spit or sand waves. Diffusive abandonment occurs when erosion is focused around the river mouth. Larger wave asymmetry leads to a discontinuity on the downdrift shoreline, which can extend during abandonment and lead to erosion. A spit abandonment arises when historical bedload is such that high downdrift wave approach angles are attained. The last mode is characterized by a culmination of downdrift migrating sandwaves and flying spits. Lobe abandonment has shaped the Ebro delta. High fluvial dominance creates conditions leading to the development of spits after lobe abandonment. The shape of these spits is the result of interaction between the new and abandoned lobes.

(ii) Modeling of time-periodic variation in sediment supply shows that it can drastically alter delta development and deposition. Signals in sediment input can force their frequency on downdrift autogenic instability. Due to differences in sand wave celerity, self-organization takes place that can shred a climate signal. Long-term monsoonal variation is believed to have shaped the Godavari delta. These fluctuations result in concave beach ridges updrift and lagoon formation in downdrift deposits. Updrift shoreline stability results in a fairly simple linear translation of fluvial sediment supply to morphology. Unstable shoreline responds makes this translation downdrift difficult.

Changes in riverine sediment input rework a deltaic shoreline. Several feedbacks between the shoreline and its reworking wave climate create a wide range in potential developments. Understanding these conditions helps determine the style and results of historical, current and future delta evolution.

10.1 Outlook

Clearly the highest priority for further research is validation of the hypotheses posed in this report. Since this is purely a modeling study, comparison with the reconstructed evolution of natural deltas could provide a necessary affirmation. Out of the complexity of deltaic behavior, this model simulated one feedback. Before introducing new processes into this model, such as sea level variability, tides, or complex fluvial dynamics, it would be more appropriate to first investigate and validate feedbacks inherent in those processes and their relation with plan-view delta development.

11 Acknowledgements

I would like to thank everyone who gave me the possibility to complete my thesis. I am deeply indebted to my supervisor Andrew Ashton, whose help, stimulating discussions and encouragements helped me before, during and after stay in Woods Hole. I greatly appreciate Pieter Roos, who put me in contact with Andrew, and whose enthusiasm and knowledge helped me allot during the difficult first months in Holland. I thank Liviu Giosan and Suzanne Hulscher for all their help.

Finally I'd like to thank my friends for the great time I had the past couple months. I enjoyed everything Woods Hole still reminds me of; from soccer to (the) softball and seminars to all the amazing people I've met. Nights at the beach, hockey games with friends and trips to Boston and New York City. In particular I'd like to thank Koen, Alje, Bert and Reinier for helping me explore the wealth of fun things in life.

12 References

Anderson, R. S., and S. P. Anderson (2011), *Geomorphology: the mechanics and chemistry of landscapes*, Cambridge Univ. Press, Cambridge, UK.

Ashton, A. D., and A. B. Murray (2006a), High-angle wave instability and emergent shoreline shapes: Wave climate analysis and comparisons to nature, *J. Geophys. Res.*, *111*.

Ashton, A. D., and A. B. Murray (2006b), High-angle wave instability and emergent shoreline shapes: Modeling of sand waves, flying spits, and capes, *J. Geophys. Res.*, *111*.

Ashton, A. D., and L. Giosan (2011), Wave-angle control of delta evolution, *Geophys Res Lett*.

Ashton, A. D., A. B. Murray, and O. Arnoult (2001), Formation of coastline features by large-scale instabilities induced by high-angle waves, *Nature vol. 414*, 296-300, 666.

Ashton, A. D., A. B. Murray, and R. Littlewood (2007), The response of spit shapes to wave-angle climates.

Ashton, A. D., L. Giosan, and A. Kettner (2010), Project Summary: investigating Human and Climate Influences on Delta Evolution Using Fluvial Discharge and Coastal Evolution Models, *Funding Proposal Rep.*, NSF-EAR.

Bakker, W. T. J. N. P., and T. Edelman (1965), The Coastline of River-deltas, in *Coast Eng*, edited, Rijkswaterstaat, The Hague.

Bates, C. C. (1953), Rational theory of delta formation, *AAPG Bulletin*, 2119-2162.

Bhattacharya, J. P., and L. Giosan (2003), Wave-influenced deltas: geomorphological implications for facies reconstuction, *Sedimentology*, 187-210.

Bolanos, R., G. Jorda, J. Cateura, J. Lopez, J. Puigdefabregas, J. Gomez, and M. Espino (2009), The XIOM: 20 years of a regional coastal observatory in the Spanish Catalan coast, *Journal of Marine Systems*, *77*(3), 237-260.

Canicio, A., and C. Ibanez (1999), The Holocene Evolution of the Ebro Delta Calalonia, Spain, *Acta Geographica Sinica*, *54*(5), 462-469.

Cavaleri, L. (2005), The wind and wave atlas of the Mediterranean Sea - the calibration phase, *Adv. Geosci.*, *2*, 255-257.

Cook, E. R., K. J. Anchukaitis, B. M. Buckley, R. D. D'Arrigo, G. C. Jacoby, and W. E. Wright (2010), Asian Monsoon Failure and Megadrought During the Last Millennium, *Science*, *328*(5977), 486-489.

Dalrymple, R. W., B. A. Zaitlin, and R. Boyd (1992), Estuarine Facies Models - Conceptual Basis and Stratigraphic Implications, *J Sediment Petrol*, *62*(6), 1130-1146.

de Vriend, H. J., M. Capobianco, T. Chesher, H. E. de Swart, B. Latteux, and M. J. F. Stive (1993), Approaches to long-term modellling of coastal morphology: a review, *Coastal Eng.*, *21*, 225-269.

Edmonds, D. A., and R. L. Slingerland (2007), Mechanics of river mouth bar formation: Implications for the morphodynamics of delta distributary networks, *J Geophys Res-Earth*, *112*(F2), -.

Edmonds, D. A., and R. L. Slingerland (2010), Significant effect of sediment cohesion on delta morphology, *Nature Geoscience*, *3*(2), 105-109.

Ericson, J. P., C. J. Vorosmarty, S. L. Dingman, L. G. Ward, and M. Meybeck (2006), Effective sea-level rise and deltas: Causes of change and human dimension implications, *Global and Planetary Change*, *50*(1-2), 63-82.

Fagherazzi, S. (2008), Self-organization of tidal deltas, *PNAS*, *105*(48), 18692-18695.

Falqués, A., and D. Calvete (2005), Large-scale dynamics of sandy coastlines: Diffusivity and instability, *J. Geophys. Res.*, C03007.

Fraticelli, C. M. (2006), Climate forcing in a wave-dominated delta: The effects of drought-flood cycles on delta progradation, *Journal of Sedimentary Research*, *76*(9-10), 1067-1076.

Galloway, W. D. (1975), Process Framework for describing the morphologic and stratigraphic evolution of deltaic depositional systems, in *Deltas Models for Exploration*, edited, pp. 87-89.

Giosan, L. (2007), Morphodynamic feedbacks on deltaic coasts: Lessons form the wave-dominated Danube delta, paper presented at Coastal Sediments '07.

Giosan, L., J. P. Donnelly, S. Constantinescu, F. Filip, I. Ovejanu, A. Vespremeanu-Stroe, E. Vespremeanu, and G. A. T. Duller (2006), Young Danube delta documents stable Black Sea level since the middle Holocene: Morphodynamic, paleogeographic, and archaeological implications, *Geology*, *34*(9), 757-760.

Grijm, W. (1964), Theoretical forms of shorelines, paper presented at IXth Conference on Coastal Engineering, Lisbon.

Guillen, J., and J. Jimenez (1995), Processes behind the Longshore Variation of the Sediment Grain Size in the Ebro Delta Coast, *Journal of Coastal Research*, *11*(1), 205-218.

Hoogendoorn, R. M., I. Overeem, and J. E. A. Storms (2008), Process-response modelling of fluvio-deltaic stratigraphy, *Computers & Geosciences*, 1394-1416.

Huh, O. K., J. M. Coleman, D. Braud, and L. Kiage (2004), Appendix A: The Major River Deltas Of the World*Rep.*, LSU, Baton Rouge, LA, USA.

Ibanez, C., A. Canicio, J. W. Day, and A. Curco (1997), Morphologic Development, Relative Sea Level Rise and Sustainable Management of Water and Sediment in the Ebro Delta, Spain, *Journal of Coastal Conservation*, *3*(2), 191-202.

Jerolmack, D. J., and J. B. Swenson (2007), Scaling relationships and evolution of distributary networks on wave-influenced deltas, *Geophys Res Lett*, *34*(23), -.

Jerolmack, D. J., and D. Mohrig (2007), Conditions for branching in depositional rivers, *Geology*, *35*(5), 463-466.

Jerolmack, D. J., and C. Paola (2010), Shredding of environmental signals by sediment transport, *Geophys Res Lett*, *37*, -.

Jimenez, J. A., and A. Sanchez-Arcilla (1993), Medium term coastal response of the Ebro delta, Spain, *Marine Geology*, 105-118.

Jimenez, J. A., A. Sanchez-Arcilla, H. I. Valdemoro, V. Gracia, and F. Nieto (1997), Processes reshaping the Ebro delta, *Marine geology*, *144*(1-3), 59-79.

Komar (1998), *Beach processes and sedimentation*, 2 ed., Prentice-Hall, Upper Saddle River.

Komar, P. D. (1973), Computer models of delta growth due to sediment input from rivers and longshore transport, *GSA Bulletin*, 2217-2226.

Milliman, J. D., K. L. Farnsworth, P. D. Jones, K. H. Xu, and L. C. Smith (2008), Climatic and anthropogenic factors affecting river discharge to the global ocean, 1951-2000, *Global and Planetary Change*, *62*(3-4), 187-194.

Murray, A. B. (2003), Contrasting the goals, strategies and predictions associated with simplified numerical models and detailed simulations, *Prediction in geomorphology, geophysical monograph vol.135*, 1-15.

Murray, A. B., and A. D. Ashton (2004), Extending a 1-line modelling approach to explore emergent coastline behaviours, paper presented at Coast Eng, Lisbon.

Nageswara Rao, K., N. Sadakata, B. Hema Malini, and K. Taka Yasu (2005), Sedimentation processes and asymmetric development of the godavari delta, India, *SEPM Special Publication*, *83*.

Nageswara Rao, K., P. Subraelu, K. C. V. Naga Kumar, G. Demudu, B. Hema Malini, A. S. Rajawat, and Ajai (2010), Impacts of sediment retention y dams on delta shoreline recession: evidences from the Krishna and Godavari deltas, India, *Earth Surf. Process. Landforms*, *1977*.

NASA (2000), Landsat program, edited, USGS.

NOAA (2011), NOAA wavewatch III, edited.

Orton, G. J., and H. G. Reading (1993), Variability of deltaic processes in terms of sediment supply, with particular emphasis on grain size, *Sedimentology*, 475-512.

Pranzini, E. (2001), Updrift river mouth migration on cuspate deltas: two examples from the coast of Tuscany (Italy), *Geomorphology*, 125-132.

Ratsimandresy, A. W., and M. G. Sotillo (2003), Reanalisis de 44 anos (1958-2001) del clima oceanico y atmosferico en el Mar Mediterraneo: Informe tecnico de la contribucion de Puertos del Estado al proyecto europeo HIPOCAS*Rep.*, 397 pp, Madrid, Spain.

Roberts, H. H. (1997), Dynamic changes of the Holocene Mississippi River delta plain: The delta cycle, *Journal of Coastal Research*, *13*(3), 605-627.

Rowland, J. C., W. E. Dietrich, and M. T. Stacey (2010), Morphodynamics of subaqueous levee formation: Insights into river mouth morphologies arising from experiments, *J. Geophys. Res.*, *115*(F4), F04007.

Sanchez-Arcilla, A., J. A. Jimenez, and H. I. Valdemoro (1998), The Ebro delta: Morphodynamics and vulnerability, *Journal of Coastal Research*, *14*(3), 754-772.

Sanchez-Arcilla, A., J. A. Jimenez, M. J. F. Stive, C. Ibanez, N. Pratt, J. W. Day, and M. Capobianco (1996), Impacts of sea-level rise on the Ebro Delta: A first approach, *Ocean Coast Manage*, *30*(2-3), 197-216.

Suter, J. R. (1997), Deltaic coasts, in *Coastal evolution*, edited, pp. 87-121, Cambridge University Press, Cambridge, UK.

Syvitski, J. P. M., and Y. Saito (2007), Morphodynamics of deltas under the influence of humans, *Global and Planetary Change*, *57*, 261-282.

Syvitski, J. P. M., et al. (2009), Sinking deltas due to human activities, *Nature Geoscience*, *Progress article*.

Thorndycraft, V. R., and G. Benito (2006), Late Holocene fluvial chronology of Spain: The role of climatic variability and human impact, *CATENA*, *66*(1-2), 34-41.

Vella, C., T.-J. Fleury, G. Raccasi, M. Provansal, F. Sabatier, and M. Bourcier (2005), Evolution of the Rhone delta plain in the Holocene, *Marine geology*, *222-223*, 235-265.

Vericat, D., and R. J. Batalla (2006), Sediment transport in a large impounded river: The lower Ebro, NE Iberian Peninsula, *Geomorphology*, *79*(1-2), 72-92.

Wright, L. D. (1977), Sediment Transport and Deposition at River Mouths - Synthesis, *Geol Soc Am Bull*, *88*(6), 857-868.